Chapter 4

Simulation results in Hydrogen

Parallel plate reactors are often used for reactive ion etching (RIE) processes. The reactor is used to produce a plasma of a molecular gas, such as SF_6 or CH_4, depending on the material to be etched. The gas is dissociated in the plasma to provide reactive neutral species (e.g., F or H) which can chemically react with the substrate to perform the etching, and also provides a source of energetic ions to drive the etching process (the role of the ions is discussed in Section 4.6). RIE is used as part of the production technique for many different micro-technologies, just a few examples include production of trench capacitors; planar, buried or ridge semi-conductor lasers and optical splitters. As microelectronic technologies become increasingly sophisticated more device components are included per circuit, which necessitates making each device smaller and packing them closer together. This requires extremely good control of parameters such as uniformity of the plasma density across the whole wafer; the energy and angular distributions of ions at the substrate surface; and ion and neutral fluxes. To accomplish this it is critical to have a good understanding of the plasma response to a wide range of running conditions.

Recent work suggests that the ion energy distribution at the substrate is critical in determining etching rates in RIE processing of SiO_2 (Perry (1994)) and also influences film properties in deposition processes (Ichiki, Momose and Yoshida (1994)). Fast etching rates are important for economical production of wafers since faster etching gives a faster turn-around on processing time. However conditions which produce fast etching are also conducive to substrate damage and so a balance must be maintained between etching rates and damage. Average plasma potentials determine the average energy of ions at the substrate, but rf effects can lead to ions arriving with much larger or smaller energies. Hence it is extremely important to determine the ion energy distribution function (IEDF) at the powered electrode surface, where the substrate is normally placed. Unfortunately this is a difficult experiment to perform, due to the large, time-dependent voltages on the electrode. Simulations are an ideal method of determining the dependence of parameters, such as the ion EDF, on a variety of externally determined variables, including the applied voltage, area ratio, source frequency, and background gas pressure.

4.1 Plasma Potentials

Knowledge of the average sheath potentials is essential in determining the average energy of collisionless ions at the electrodes. To determine the sheath potentials it is first necessary to examine the temporal variation of the potential across the whole plasma. In Figure 4.1 the plasma potential is plotted as a function of position for various area ratios

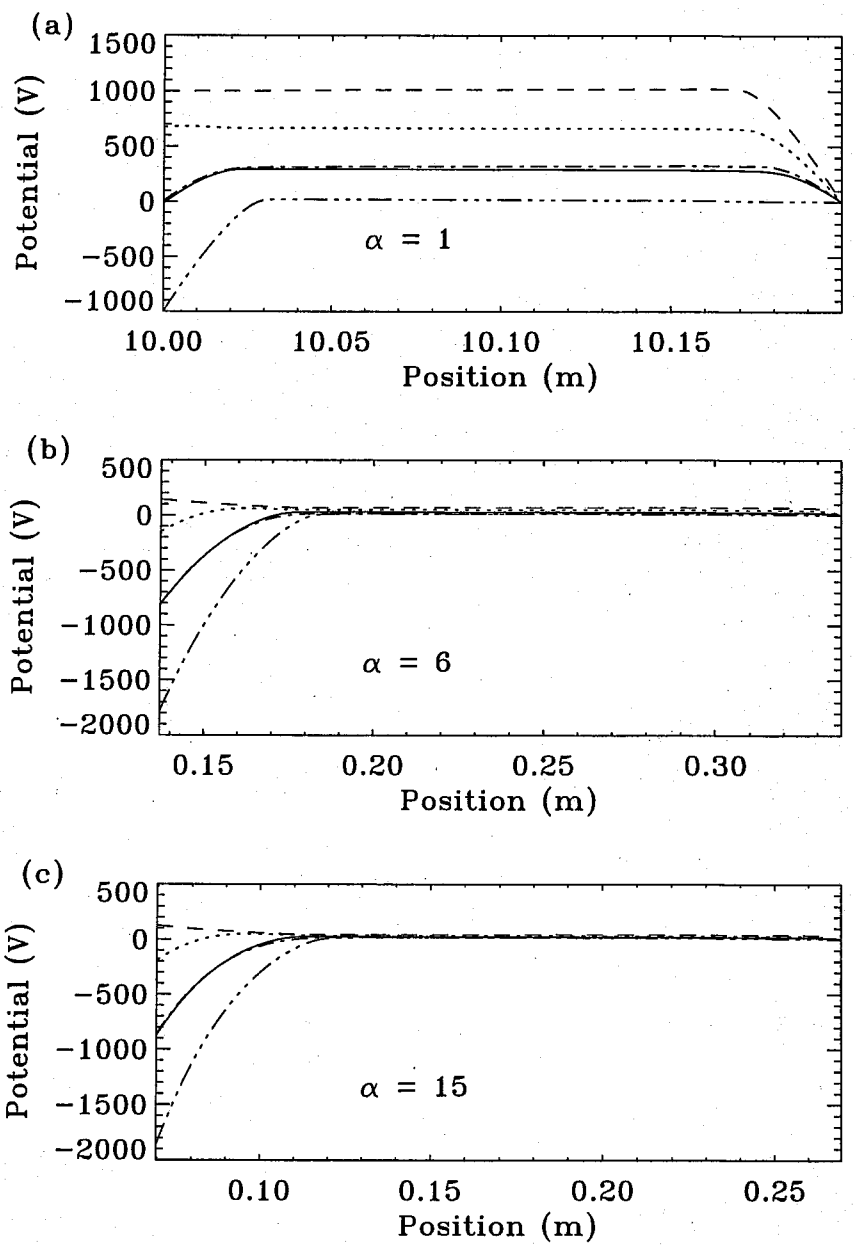

Figure 4.1 Potential profiles across the plasma at phases $\omega t = 0$ (solid line), $\pi/4$ (dotted line), $\pi/2$ (dashed line), π (dash-dot line), $3\pi/2$ (dash-3 dots) for area ratios **(a)** $\alpha = 1$, **(b)** $\alpha = 6$ and **(c)** $\alpha = 15$.

at phases – ωt = 0, $\pi/4$, $\pi/2$, π and $3\pi/2$. These plots clearly demonstrate that most of the potential variation occurs in the sheath regions and that potential gradients in the bulk are small. For each different geometry the simulations are run with an applied voltage amplitude of 1 kV and a frequency of 10 MHz, with a background gas pressure of 20 mTorr and collisionless ions. In Figure 4.2 both the live and ground *sheath* potentials are

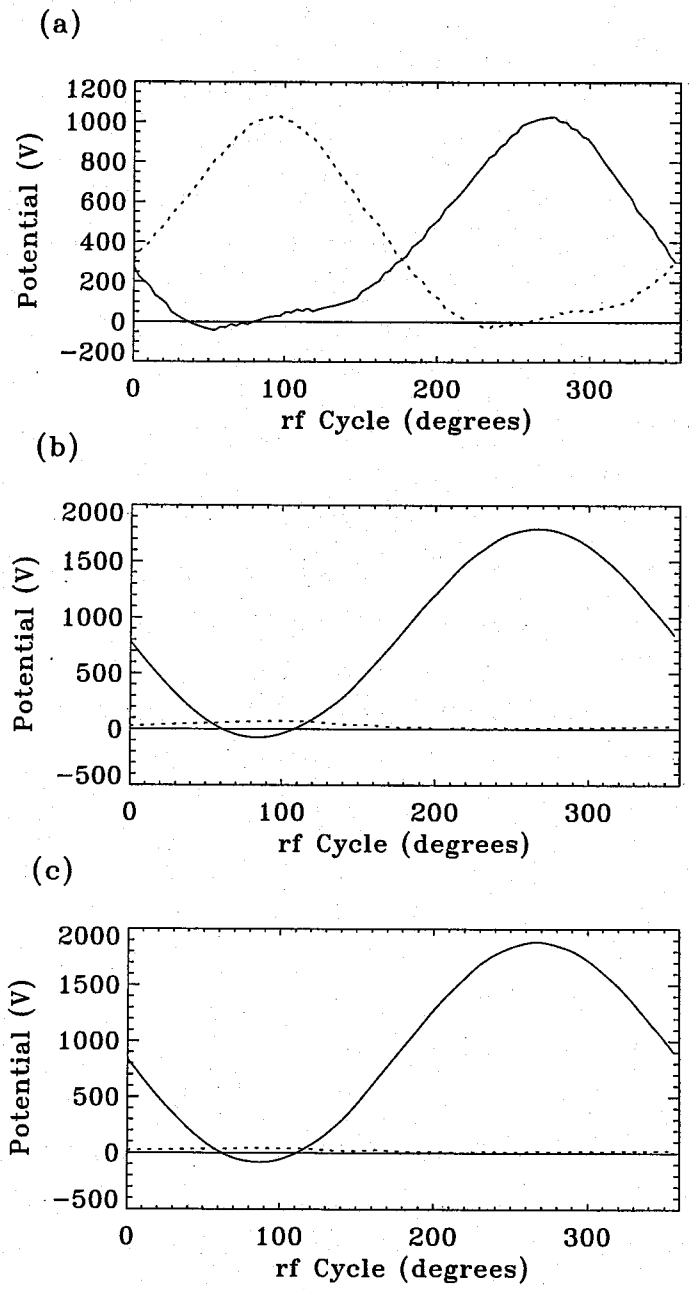

Figure 4.2 Sheath potentials as a function of the rf phase for the live (solid line) and grounded sheath (dotted line). The sheath potential is the difference between the bulk and electrode potentials. Results are shown for area ratios **(a)** $\alpha = 1$, **(b)**$\alpha = 6$ and **(c)** $\alpha = 15$.

shown for the same set of conditions. The sheath potential is defined as the electrode potential measured relative to the potential in the centre of the plasma and hence is a measure of the magnitude of the voltage drop from the centre of the plasma to the electrode. Figure 4.1 (a) shows conditions for the symmetric system, $\alpha = 1$ – the applied potential on the live electrode varies periodically between 1000V at $\omega t = \pi/2$ and -1000V at $\omega t = 3\pi/2$ at the live electrode. The symmetry of the system can be seen even more clearly in Figure 4.2 (a) – both live and grounded sheath potentials vary sinusoidally between 0 and 1000V in identical fashion with a phase separation of 180°. In effect they are mirror images of each other. The wobble in the curves close to zero sheath potential is due to the incursion of electrons during the period when the sheath is collapsed; this is discussed in detail in Section 4.3. As α is increased (i.e., the area of the grounded electrode increases relative to the live electrode) the distribution of voltage between the sheaths becomes increasingly asymmetric. Looking at the potential plots in both Figures 4.1 and 4.2 for cases (b) $\alpha = 6$ and (c) $\alpha = 15$, almost all of the voltage is dropped across the live sheath and only a small fraction across the grounded sheath.

From Figure 4.1 it can also be seen that as α is increased the potential at the live electrode develops an increasingly negative dc offset – this is known as the bias voltage, V_{bias}. The bias voltage develops because the circuit capacitor charges up negatively in the first few microseconds of running the simulation. This limits the maximum excursion of the voltage on the live electrode, which in turn reduces the peak value of the bulk plasma potential; this is represented schematically in Figure 4.3. As the area ratio increases the bias voltage becomes more negative and a larger percentage of the total voltage is dropped at the live electrode, leading to a large disparity in the average live and ground voltages. From Figures 4.1 (b) and (c) it can be seen that for $\alpha = 6$ and $\alpha = 15$, with respective bias voltages of -825 V and -880 V (i.e., $|V_{bias}| \approx V_{rf}$), almost the full 2000 V peak-to-peak voltage is dropped across the live sheath. The magnitude of the bias voltage depends in a complex fashion on the area ratio of the electrodes and the sheath densities; the derivation is presented in the next section.

Another way of viewing the difference in magnitude of the voltages dropped across each sheath is presented in Section 3.3.3. Briefly it models the plasma as an electric circuit with the sheaths acting as two capacitors in series. The sheath capacity is proportional to the area of the sheath divided by the maximum sheath width, where the sheath area can be approximated by the electrode area. For asymmetric systems the live electrode area is smaller than that of the grounded electrode resulting in a smaller live sheath capacitance (at high area ratios it can be an order of magnitude less than the grounded sheath capacitance), and so there will be a larger rf voltage across the live sheath.

One other important point to note from Figure 4.1 is that for area ratios > 1 the

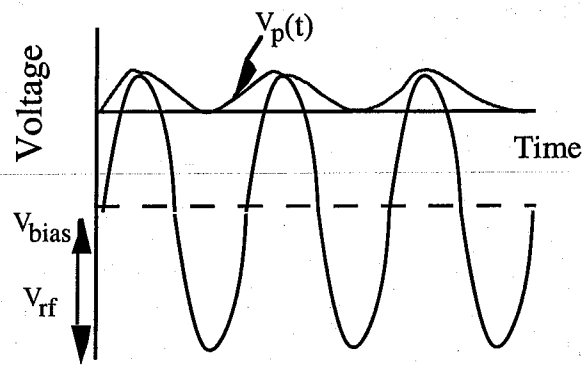

Figure 4.3 Schematic of the applied voltage at the live electrode as a function of rf cycle, demonstrating the decrease in the bulk plasma potential due to the creation of a negative bias voltage.

electrode potential can transiently reach values which are much larger than the bulk potential, as the wall potential rises the plasma potential lags behind, creating a field reversal at the wall. This can also be seen in Figure 4.2, in the period when the sheath potential becomes negative. For area ratios of 6 or more the live electrode potential can reach values twice that of the bulk potential at $\omega t = \pi/2$. Electrons in the vicinity of the field reversal are accelerated out to the wall, enhancing electron losses from the bulk. As more electrons are lost the plasma potential rises and loss rates decrease. The electron current to the wall during the period of sheath collapse must be sufficient to balance the total ion current for the whole cycle. Field reversal and the formation of beam-like electron distributions (discussed in Section 4.3) are two mechanisms by which this is accomplished.

4.1.1 Ratio of live to ground sheath potential

The ratio of the average sheath potentials at the live and grounded electrodes as a function of the electrode area ratio is an important parameter in asymmetric systems. For simulations in which ions make no collisions this directly determines the ratio of average ion energies at each electrode. In RIE reactors the substrate is generally placed at the powered electrode and so the average ion energy at this position will affect the processing. Figure 4.6 (a) shows a plot of the voltage ratio as a function of area ratio for collisionless ions and 4.6 (b) the same for collisional ions. Plotted on the same graphs are results from another spherical PIC model by Alves *et al* (1991), and from an analytic model by Lieberman (1989), which determines a relationship between the electrode areas

and the average sheath potentials of the form

$$\frac{V_a}{V_b} = \left(\frac{A_b}{A_a}\right)^q, \qquad (4.1)$$

where Lieberman determines different values for the exponent q, depending on the physics included in the bulk and sheath regions. For the collisionless ion case, $q = 1.33$, and for the collisional case $q = 1.25$. Note that Lieberman's theory is not expected to give exact agreement with the simulation since the derivation assumes ions are collisional in the bulk. However (4.1) represents a straight-forward relationship between voltage and area ratio, and it is interesting to compare to simulation results.

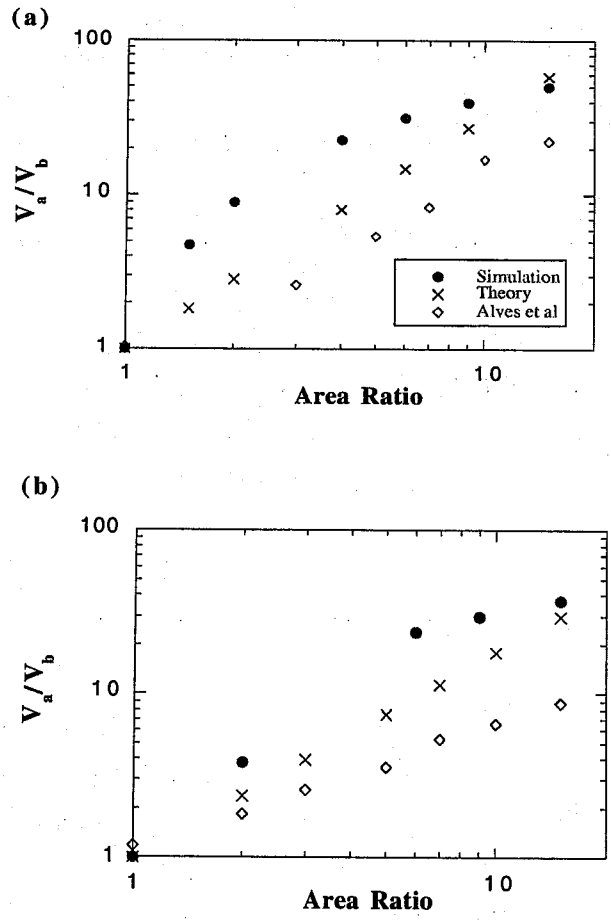

Figure 4.4 Ratio of the average live to ground sheath voltages as a function of the area ratio, showing results with **(a)** collisionless ions **(b)** ion-neutral collisions. Solid dots are results from the simulation, crosses are results from Lieberman's theory (4.1) and diamonds are results from another spherical PIC simulation (Alves *et al* (1991)).

Interestingly the two PIC simulations give quite different results even though both use similar techniques and both model an atomic hydrogen plasma; the theoretical calculations from Lieberman lie somewhere in between the two . Alves *et al* use two perpendicular velocities instead of a perpendicular energy, but this should not cause significant differences for one dimensional spherical geometry. The main difference between the simulations is that Alves *et al* run at slightly higher pressures and half the applied voltage i.e., $p = 30$ mTorr and $V_{rf} = 500$V. It would therefore seem that either, or both, voltage and pressure are important in determining the voltage division, even though this is not accounted for in the conventional theories. The Alves results and the theory both predict a power-law dependence on the area ratio, but results in this thesis show a definite saturation at higher area ratios, indicating that the ratio of the average sheath voltages does not follow a simple power-law dependance on the ratio of the electrode areas. The main effect of adding collisions seems to be to slightly lower the voltage ratio for all results.

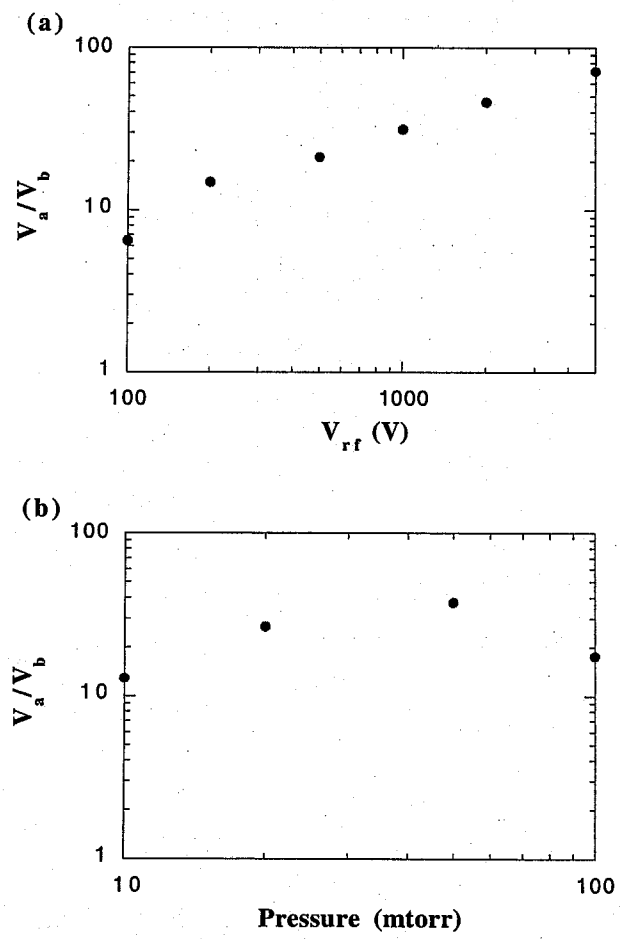

Figure 4.7 Voltage ratio for collisionless ions as a function of **(a)** applied voltage at $p = 20$ mTorr and **(b)** pressure at $V_{rf} = 1$ kV, for a constant area ratio $\alpha. = 6$.

To determine the effect of applied voltage and pressure on the ratio V_a/V_b (for collisionless ions) results are plotted in Figure 4.7 (a) and (b) respectively for a constant area ratio of $\alpha = 6$. There is obviously a strong power-law dependence on the applied voltage, with the form $V_a/V_b \propto V_{rf}^{0.6}$. The dependance on pressure is more complex, appearing to peak at intermediate pressures. Obviously, according to these results, the voltage ratio depends on V_{rf} and p, and is not solely a function of the electrode area ratio. All theoretical calculations of the voltage ratio known to the author (Koenig and Maissel (1970), Coburn and Kay (1972), Logan *et al* (1977), Keller and Pennebaker (1979), Horowitz(1983), Lieberman (1988), Song *et al* (1990), Raizer and Shneider (1992)), including the equation used to compare to the simulation results in Figure 4.6, were determined using this assumption, indicating an over-simplification of the physics in the derivation.

4.1.2 Bias Voltage Calculation

This section looks at how the bias voltage is determined from the applied voltage and the area ratio. The derivation follows a similar method to that used by Meijer (1991). An equation relating the voltages across the system can be determined from Kirchoff's law

$$V_b(t) - V_a(t) = V_{bias} + V_{rf}\sin\omega t\,, \qquad (4.2)$$

where V_a and V_b are the voltage drops across the live and ground sheaths respectively, and V_{bias} is the dc bias voltage at the live electrode. At time $\omega t = \pi/2$ the sheath at the live electrode collapses (i.e., $s_a = 0$), so assuming that the electrode potential is *always less than or equal* to the plasma potential, the sheath potential at the live electrode should be approximately zero, $V_a \approx 0$. Similarly at time $\omega t = 3\pi/2$, the ground sheath collapses and $V_b \approx 0$, thus giving two linked equations for the sheath potentials. Writing (4.2) in terms of the normalised potential, $\eta = e\phi/kT_e$ gives

$$\eta_b = \eta_{rf} + \eta_{bias} \qquad \text{at } \omega t = \pi/2, \qquad (4.3)(a)$$

and

$$-\eta_a = -\eta_{rf} + \eta_{bias} \qquad \text{at } \omega t = 3\pi/2. \qquad (4.3)(b)$$

In order to obtain the sheath potential as a function of the position in the sheath the sheath equation derived in Section 3.1.3 is used. Taking equation (3.25), expanding β and ignoring higher order terms of z gives

$$\eta = \left(\frac{9}{10}\right)^{2/3}\left(\frac{2e^2 n_o \chi r_{elec}^{5/2}}{\varepsilon_o m_i u_B{}^2 \sqrt{s}}\right)^{2/3}\left(\frac{s}{r_{elec}}\right)^{5/3}. \qquad (4.4)$$

Re-arranging (4.4) the normalised potential can be written in terms of the normalised sheath width, $\varsigma = s/\lambda_D$, where λ_d is the debye length = $\sqrt{\frac{ne^2}{m_e \varepsilon_o}}$

$$\eta = \varsigma^{4/3}\left(\frac{18\chi}{5}\right)^{2/3}, \qquad (4.5)$$

where χ is the average percentage of the cycle that the sheath exists at the electrode; from Section 3.2 $\chi = 0.85$.

From Section 4.4 a quantity s_O, the sum of the live sheath and the grounded sheaths weighted by area and sheath density ratios, is found to be independent of the rf cycle and is given by equation (4.15). Re-writing this using normalised sheath widths gives the equation

$$\varsigma_a + \alpha\frac{n_b}{n_a}\varsigma_b = \varsigma_o. \qquad (4.6)$$

where ς_a and ς_b are the normalised sheath widths at the live and grounded electrodes. Now at $\omega t = \pi/2$ the live sheath is collapsed so $\varsigma_a = 0$, and similarly at $\omega t = 3\pi/2$ $\varsigma_b = 0$, so from (4.6)

$$\varsigma_b = \frac{n_a}{\alpha n_b}\varsigma_o \qquad \text{at } \omega t = \pi/2, \qquad (4.7)(a)$$

and

$$\varsigma_a = \varsigma_o \qquad \text{at } \omega t = 3\pi/2 \qquad (4.7)(b)$$

Substituting (4.5) into (4.3)to determine the normalised sheath potentials in terms of the bias and rf voltages, and using (4.7) to swap ς_a and ς_b for ς_o gives the equations

$$\left(\frac{n_a \varsigma_o}{n_b \alpha}\right)^{4/3}\left(\frac{18\chi}{5}\right)^{2/3} = \eta_{rf} + \eta_{bias} \qquad \text{at } \omega t = \pi/2, \qquad (4.8)(a)$$

and

$$\varsigma_o{}^{4/3}\left(\frac{18\chi}{5}\right)^{2/3} = \eta_{rf} - \eta_{bias} \qquad \text{at } \omega t = 3\pi/2 \qquad (4.8)(b)$$

Solving (4.8) (a) and (b) simultaneously the normalised bias voltage can be found as a function of the area ratio and the sheath densities.

$$\eta_{bias} = -\left(\frac{\alpha^{4/3} - \left(\frac{n_a}{n_b}\right)^{4/3}}{\alpha^{4/3} + \left(\frac{n_a}{n_b}\right)^{4/3}} \right) \eta_{rf} \qquad (4.9)$$

From the simulation the maximum value for n_a/n_b is found to be 1.5 at $\alpha = 15$. By approximating the bias voltage using $n_a/n_b = 1$, η_{bias} can be written solely as a function of the area ratio

$$\eta_{bias} \approx -\left(\frac{\alpha^{4/3} - 1}{\alpha^{4/3} + 1} \right) \eta_{rf} \qquad (4.10)$$

Normalised bias potentials calculated from equations (4.9) and (4.10) are converted to real values (by multiplying by the electron temperature) and plotted in Figure 4.8 (a) for collisionless ions, along with the simulation values and the results published by Meijer. Meijer's results are determined by solving sheath equations analytically as far as possible, and then using numerical integration techniques to solve the final equations. The correspondence between equation (4.9) and the simulation is remarkably good, fitting to within 10%. The values calculated using equation (4.10) are too low at small area ratios but correspond well to Meijer's numerical results, which are derived assuming equal densities in both sheaths. Interestingly the assumption that the electrode potential is always less than the bulk potential does not appear to have much effect on the accuracy of the bias voltage derivation. Possibly this is because the amount by which the electrode voltage exceeds the bulk potential is small relative to the maximum sheath potential, even at high area ratios.

The bias voltage for collisional ions is plotted in Figure 4.8 (b) showing results from the simulation and the theoretical curves from (4.9) and (4.10). Meijer did not present results including ion collisions. Interestingly this shows that results from the simulation have dropped significantly at $\alpha = 2$, but changed relatively little for higher area ratios. Lack of further data at small area ratios makes it difficult to determine the extent of the differences between collisionless and collisional simulations. The theoretical curve from (4.9) also still fits well at high area ratios but is much too low at $\alpha = 2$. The curve calculated from (4.10) has, of course, remained constant, since it depends only on area ratio. The fact that equation (4.9) does not accurately predict the bias voltage for $\alpha = 2$ is most likely due to the derivation, since the normalised sheath equation (4.4) was determined assuming collisionless ions. This is apparently not so important at higher area ratios, possibly because the bias voltage "saturates" at high values making the differences smaller.

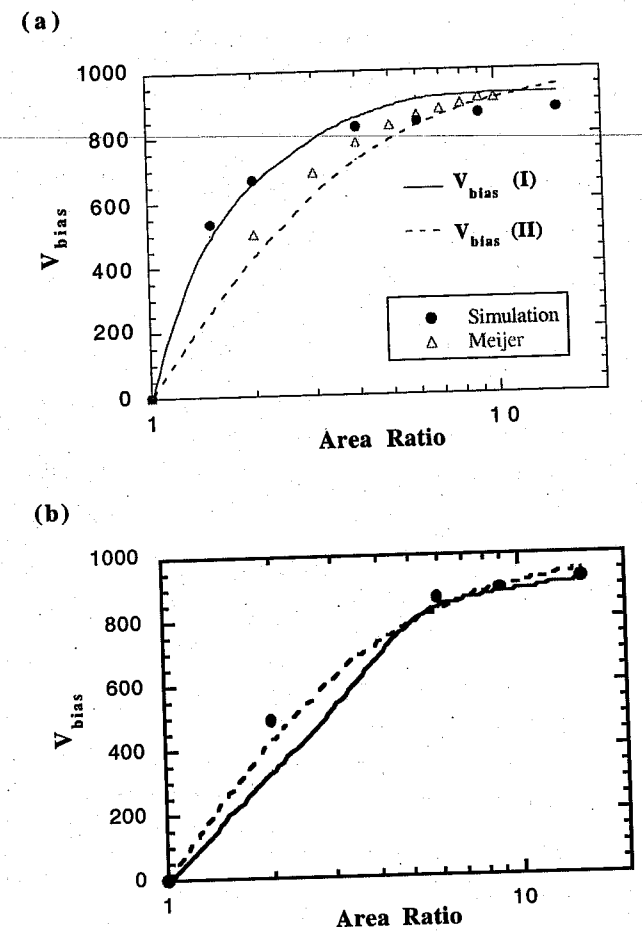

Figure 4.8 Bias voltage plotted as a function of area ratio for **(a)** collisionless ions and **(b)** collisional ions showing results from simulation (solid dots) and Meijer (hollow triangles), with theoretical curves (I) (solid line) from equation (4.9) and (II) (dotted line) from (4.10).

4.2 Rf Sheath

4.2.1 Time-dependant sheath widths

At a fixed rf frequency, the maximum sheath extension determines the velocity of the sheath since the sheath moves in phase with the applied voltage (i.e., when the voltage is increasing the sheath expands and vice versa). This is important since when the sheath velocity exceeds a critical value, the sheath motion can strongly influence the electron energy distribution in the sheath (see Section 4.2.2). The maximum extension of the electron sheath width can therefore be used in determining a rough estimate of the

energy that the electrons gain through interaction with the sheath. The sheaths move in anti-phase to one another, so when one is expanding the other is contracting.

The sheath width can be determined as a function of cycle from conservation of the total current. The total current I_{rf} is given by the sum of the conduction and convection currents, and must be equal in magnitude and opposite in direction at each electrode

$$I_{rf} = \left[i_a - e_a - A_a j_{d\_a}\right] = -\left[i_b - e_b - A_b j_{d\_b}\right], \tag{4.11}$$

where i is the ion current, e is the electron current and j_d the displacement current; subscript a refers to the inner electrode and b to the outer. Considering the moving sheath edge as a step function the displacement current at the sheath edge can be related to the sheath velocity and the ion density in the sheath by (Godyak and Sternberg (1990))

$$j_d = -en_i(x)\frac{dx}{dt} \tag{4.12}$$

where x is the phase-dependant position of the electron sheath edge. Ignoring the period for which the sheath is collapsed, assume that the displacement current is much greater than the particle currents, i.e., $Aj_d >> i - e$. Then substituting (4.12) into (4.11) gives

$$4\pi\left(r_a + x_a\right)^2 n_i(x_a)\frac{\partial x_a}{\partial t} + 4\pi\left(r_b - x_b\right)^2 n_i(x_b)\frac{\partial x_b}{\partial t} = 0. \tag{4.13}$$

where x_a and x_b are the time-dependant live sheath and grounded sheath widths respectively, r_a and r_b are the electrode radii and n_i is the ion density. The ion density in the sheath is independent of phase and approximately equal to the density at the electrode (see Figure 4.12), so equation (4.13) can be re-written as

$$\frac{dx_a}{dt} + \alpha\frac{n_b}{n_a}\left(\frac{1 - \frac{x_b}{r_b}}{1 + \frac{x_a}{r_a}}\right)^2 \frac{dx_b}{dt} = 0, \tag{4.14}$$

where n_a and n_b are the electrode ion densities (note n_a is not necessarily equal to n_b). This is a differential equation for the sheath width as a function of time. Integrating this equation over time and truncating to first-order terms, it is found that the sum of the time-dependent live sheath width and the grounded sheath width (weighted by the term on the left-hand side of equation (4.14)) is constant over the rf cycle, and is here defined as s_o

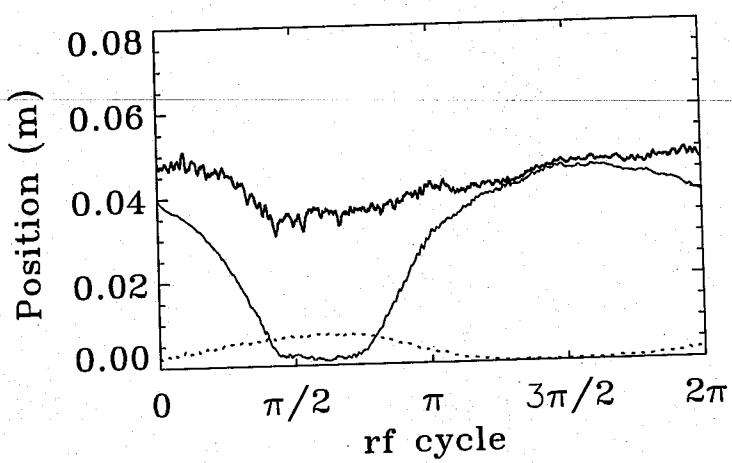

Figure 4.9 Time-dependant live (solid line) and grounded (dotted line) sheath width, and s_o from equation (4.15) (thick line), plotted as a function of the rf cycle for $\alpha = 6$. Note that s_o varies by less than 10% over the cycle.

$$x_a + \alpha\frac{n_b}{n_a}\left(\frac{1-\frac{x_b}{r_b}}{1+\frac{x_a}{r_a}}\right)x_b \approx x_a + \alpha\frac{n_b}{n_a}x_b = s_o. \tag{4.15}$$

Note that for systems in which $s_a << r_a$ and $s_b << r_b$, both x_a/r_a and $x_b/r_b \rightarrow 0$ validating the approximation on the right-hand side of equation (4.14). The second case is always true for these simulations and the first case holds well except at large area ratios (i.e., $\alpha \geq 15$). In Figure (4.9) s_o is plotted as a function of the rf cycle together with the actual individual sheath widths for $\alpha = 6$. The relationship given in (4.14) is shown to hold to within 10% variation over the cycle, even though the sum of the sheath widths varies by a much larger amount.

The maximum sheath widths can be related directly to each other, rather than through s_o, by using the assumptions that (1) the sheaths move exactly 180° out of phase with each other, and (2) during the period of collapse $s \rightarrow 0$. Therefore from equation (4.15) the sheath widths can be directly related using

$$s_a = \alpha\frac{n_b}{n_a}s_b. \tag{4.16}$$

Note that for the symmetric case equation (4.16) correctly predicts that the sheath widths will be equal. The results from this equation are plotted in Figure 4.10, in comparison

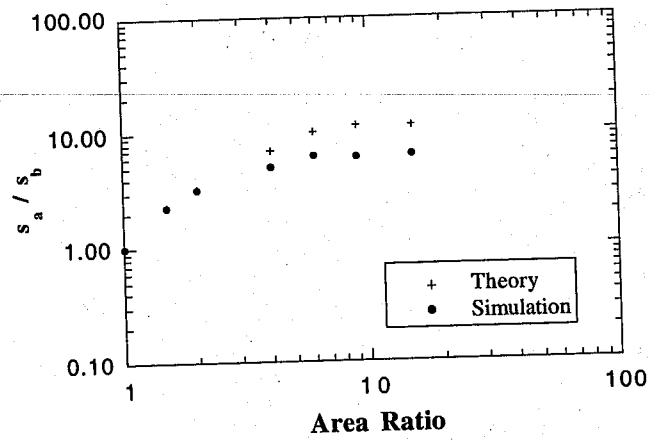

Figure 4.10 Ratio of sheath widths as a function of area ratio, with results from simulation (dots) plotted in comparison to equation (4.16)

with simulation results. Agreement is very good at small area ratios but becomes worse at higher area ratios and by $\alpha = 15$ is twice the simulation value. This is a result of neglecting the term $1 + \frac{x_a}{r_a}$ in (4.15), since at $\alpha = 15$ $s_a \approx r_a$ which introduces a factor of 0.5 to (4.16).

4.2.2 *Effect of sheath motion on electron EDF at the live electrode*

In Section 4.1 field inversion at the electrode at the time of the sheath collapse is discussed – this is one method by which electrons can be accelerated out of the plasma. Another mechanism which can enhance electron losses to the walls occurs only when the sheath motion is sufficiently rapid. For this case thermal electrons drifting into the ion sheath region are not sufficient to provide neutralisation of the ion space charge in the sheath. This drives a field reversal in the vicinity of the retreating sheath edge which accelerates electrons from the bulk toward the walls even before the sheath has collapsed, resulting in a beam-like electron velocity distribution in the sheath region. This result has been previously observed in planar PIC simulations (Surrendra and Graves (1991) and Vender and Boswell (1992)) and in a fluid model (Okuno, Ohutsu and Fujita (1992)). From Vender and Boswell a critical value for the sheath velocity is found to be

$$v_{crit} \approx \frac{1}{2}\langle v_e \rangle \qquad (4.17)$$

where $\langle v_e \rangle$ is the thermal electron velocity in the bulk. For sheath velocities less than v_{crit} the electron velocity distribution will be undisturbed, while for values greater than this the distribution will become increasingly beam-like. Enhancing electron loss rates by creating beam-like distributions in the sheath is necessary to balance the ion loss rates throughout the cycle. For a hydrogen plasma the bulk temperature is approximately 3 eV, which corresponds to a thermal velocity of $\langle v_e \rangle = 1 \times 10^6 \, \mathrm{ms}^{-1}$. Simulation results show that sheath velocities can be in excess of 3×10^6 ms^{-1}, and in some cases reach more than an order of magnitude larger than the critical sheath velocity, especially at high area ratios and applied voltages. Figure 4.11 shows the electron energy distribution at the live electrode for $\alpha = 6$ – the distribution is essentially a displaced Maxwellian and is well fitted assuming a temperature of 3 eV (dotted line), which is approximately equal to the bulk temperature. The energy offset of the beam is about 60 eV, which compares well to the negative sheath potential of -75V at $\omega t = \pi/2$ for $\alpha = 6$ (see Figure 4.2 (b)). Increased densities of energetic electrons close to the electrode in the first few microseconds of the sheath collapse have been observed experimentally for a hydrogen plasma, using the emission spectrum of the H_α line (Booth *et al* (1993)).

The energy distribution at the grounded electrode is much more complex, since some of the energetic electrons accelerated in the live sheath can traverse the plasma to reach the grounded sheath. Some electrons cross the sheath, and others are reflected depending on their energy and the phase of arrival.

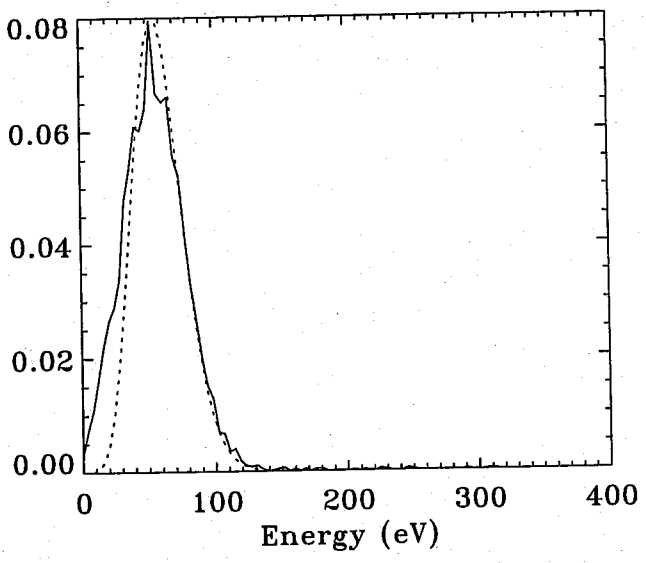

Figure 4.11 Electron energy distribution at the live electrode for $\alpha = 6$ (solid line). Also plotted is a 3 eV gaussian with a 57 eV off-set (dotted line).

The electron distribution function after the sheath has reversed and is expanding away from the electrode is also of interest. In this case inertia becomes an important factor, since electrons are not immediately expelled from the sheath region as is generally assumed. In fact it can take several nanoseconds to reverse the electron motion in the sheath, by which time the sheath potential can be very large. The inability of the electrons to immediately respond to the reversal in sheath motion initially results in cooling of the electrons – at this stage they are diffusing against the local fields and so lose energy – but a short time later electrons still in the sheath are accelerated to high energies due to the large sheath potentials. Evidence that electrons are still present in the sheath during the expansion period of the sheath can be seen in Figure 4.12, which shows the electron density as a function of position for various phases in the cycle at $\alpha = 6$. Potentials from Figure 4.2 (b) are also reproduced here for comparison. The phases $\omega t = 0 - \pi/2$ show the contraction phase of the sheath – electrons "fill in" behind the retreating sheath edge

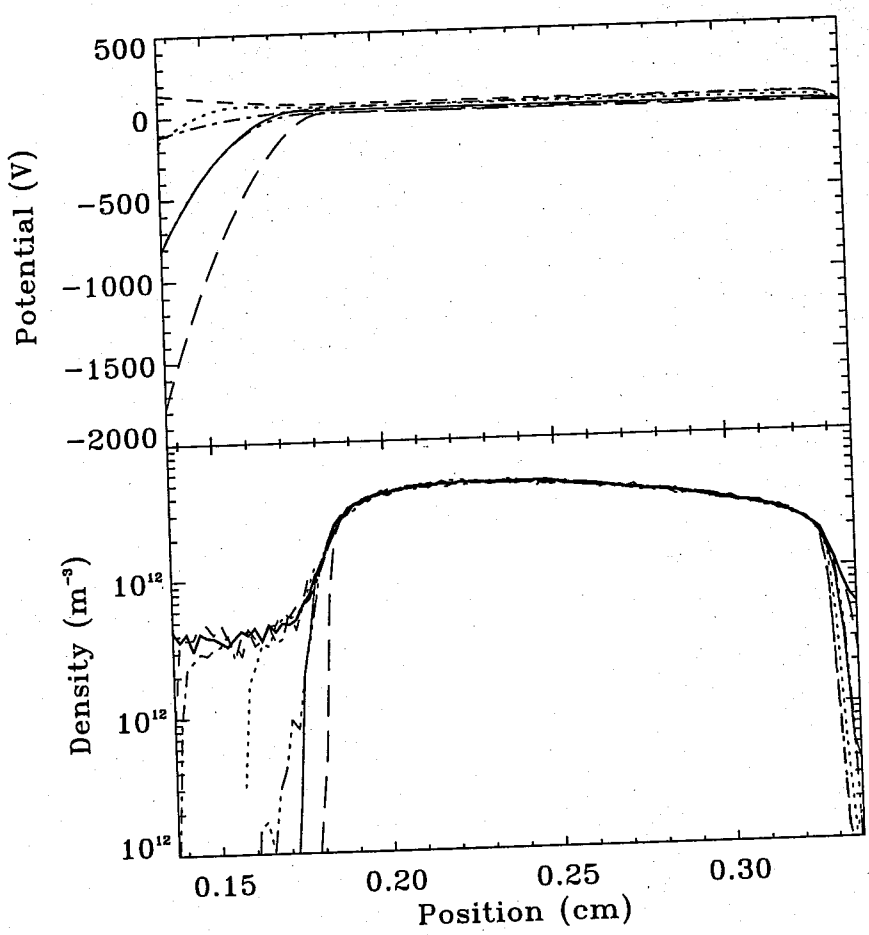

Figure 4.12 Comparison between **(a)** sheath potential and **(b)** electron density at $\omega t = 0$ (solid line), $\pi/4$ (dotted line), $\pi/2$ (dashed line), $3\pi/4$ (dash-dot line), π (dash-3 dots) and $3\pi/2$ (long dash) of the rf cycle. The thick line represents the ion density.

reaching the same density as the ions. As the sheath starts to expand again at $\omega t = \pi/2$, the electrons do not move out of the sheath as rapidly as they came in – at $\omega t = 3\pi/4$ the edge of the electron density profile is much closer to the electrode than at $\omega t = \pi/4$ and there is still a substantial electron density in the sheath even though the potential has reached -100V. At $\omega t = \pi$ the electron density in the sheath is still higher than at $\omega t = 0$, for the same potential distribution. Electrons remaining in the sheath at this time are therefore strongly accelerated by the local fields out into the bulk . This effect is therefore very important in maintaining the plasma, since the high energy electrons thus created produce enhanced ionisation rates in the bulk. This mechanism, often known as sheath or stochastic heating of the electrons, is discussed in detail in Section 4.4.2.

4.3 Plasma Current

The external circuit contains a capacitor, so no net current can flow in the system during an rf cycle; therefore currents to live and grounded electrodes must be equal and the ion and electron currents at each electrode must be equal when averaged over the cycle. Furthermore, since the plasma is a good conductor, the instantaneous rf current across the system length must be constant . Figure 4.13 (a) plots the current form at the live electrode for $\alpha = 6$, the applied voltage is plotted on the same graph. The current is basically sinusoidal in character – the fundamental harmonic from the Fourier transform is overlayed in the dotted line – but shows high frequency modulations due to higher order harmonics. The source of these oscillations in the current is discussed later in this section. The phase shift of the current relative to the potential is close to 90° indicating the plasma impedance is predominantly capacitive. The phase shift is found to be approximately constant for the entire range of area ratio, voltage, pressure and the frequency investigated, with an average value of 73°. The shift in the phase from 90° is due to an inductive component in the plasma impedance introduced by electron inertia (i.e., electrons cannot respond instantaneously to changing voltages). The components of the current at the live electrode are plotted in Figure 4.13 (b) – in the sheath the current is carried mainly by the displacement current since electrons are excluded for most of the cycle except when the sheath collapses at $\omega t = \pi/2$. The ions provide a small, constant current, independant of the rf cycle.

The current modulations indicate the presence of high frequency oscillations in the bulk electric field, and the source is attributed to the interaction of the electrons with the oscillating plasma-sheath boundary, producing standing waves in the plasma current. The effect has also been noted in planar PIC simulations (Vender (1990)

and Surrendra (1991)). As mentioned in Section 4.2.2 rapid expansion of the sheath creates a beam-like electron distribution directed into the bulk. Interaction between the high velocity electrons with the expanding sheath edge sets up a potential well in the electric field which acts to trap some of the electrons relatively close to the electrodes, increasing the probability of making an ionising collision in this region. The progression of the beam of high energy electrons from the live electrode across the plasma to the grounded electrode can be seen in Figure 4.14, a greyscale plot of the ionisation rate as a function of phase and position. Dark regions indicate enhanced ionisation, denoting the presence of electrons with energies greater than the threshold ionisation energy. Note also

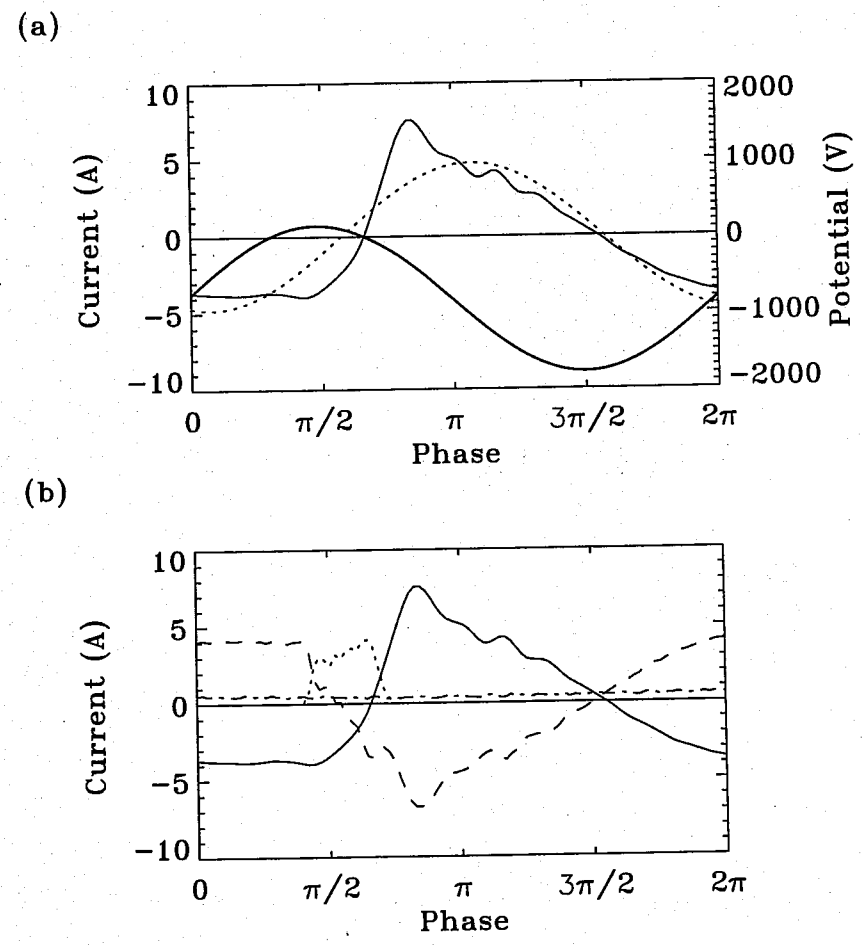

Figure 4.13 Current at live electrode as a function of phase for $\alpha = 6$.**(a)** Total current (solid line) overlaid by its fundamental harmonic (dashed line). Also plotted is the electrode potential (thick line) **(b)** Components of the total current (solid line) – displacement current (dashed line), electron current (dotted line) and ion current (dash-dotted line).

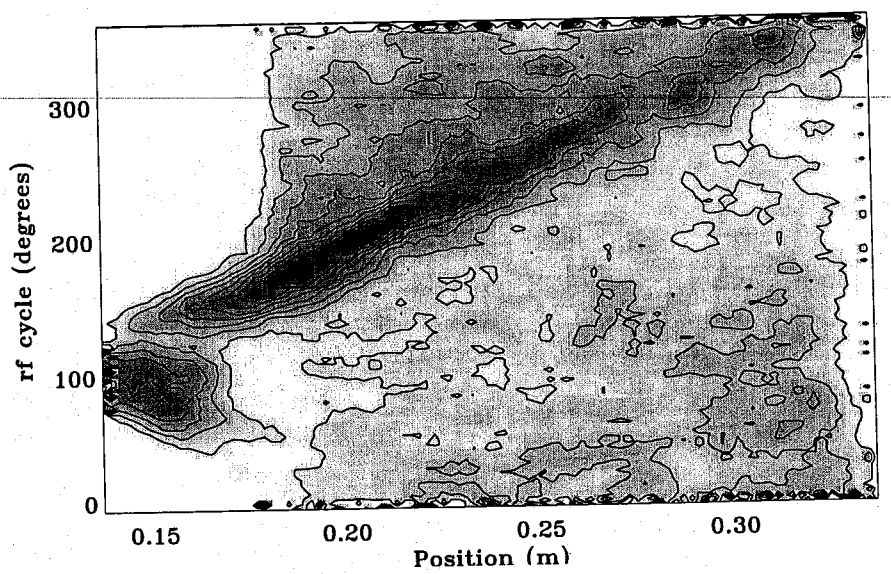

Figure 4.14 Greyscale plot of ionisation as a function of position and phase. Darkness scales linearly with increasing ionisation rate.

the presence of high-energy electrons in the live sheath as it collapses – these are accelerated toward the electrode by fields set up to balance electron and ion losses during the cycle, as discussed in Section 4.2.2.

Although the total rf current is constant across the whole plasma, the means of transmission is different in the bulk and the sheaths. In the sheath it is carried mainly by the displacement current, as previously mentioned, but in the bulk the displacement current is small and electrons are the predominant carrier; while the ion current provides little to the magnitude of the total current in either region. In the bulk, therefore, the electron current is essentially a measure of the rf current. Figure 4.15 (a) shows a 3-D graph of the electron current as a function of position and phase for the conditions $\alpha = 6$, $V_{rf} = 1$ kV and $p = 20$ mTorr. The convention used is that positive current flows in the direction of the live electrode (to the left on the graph) and negative in the direction of the grounded electrode. For $\omega t < \pi/2$, the current in the bulk is therefore flowing toward the live electrode; currents close to the live sheath edge are slightly higher due to field reversal in the sheath. At approximately $\omega t = \pi/2$ there is an increase in the electron current close to the live electrode as the electrode potential exceeds that of the bulk, then immediately afterward there is an abrupt change in the current direction as the sheath motion reverses. This creates a series of standing waves across the plasma, which quickly damp out with increasing time. These are the high frequency oscillations observed in the average live electrode current in Figure 4.13 (a). As ωt increases a series of electron beams are accelerated from the expanding sheath edge, the largest occurring just after reversal of the sheath direction when the electron density in the sheath is high

(a)

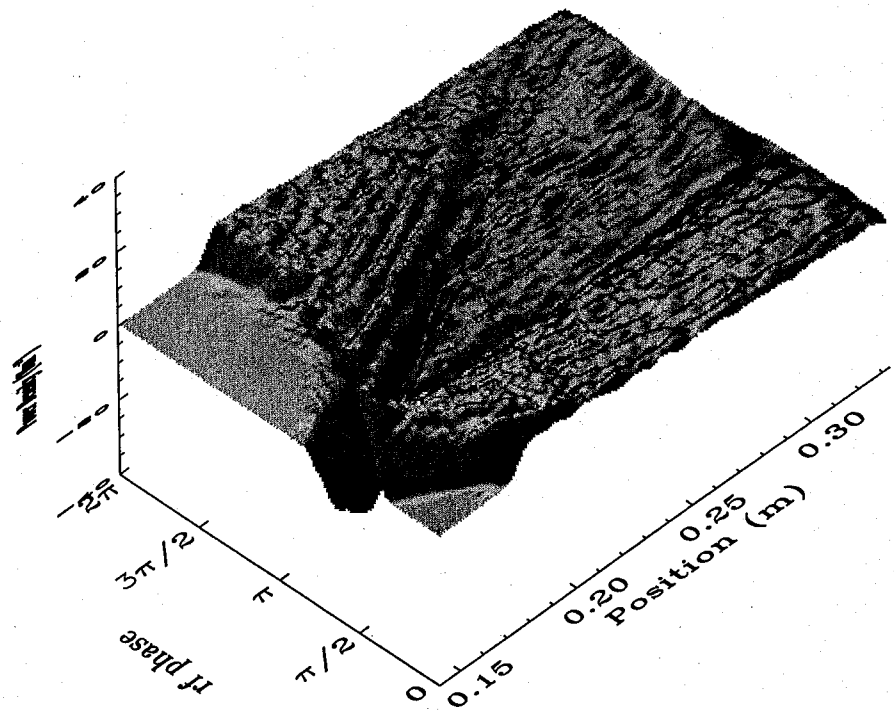

(b)

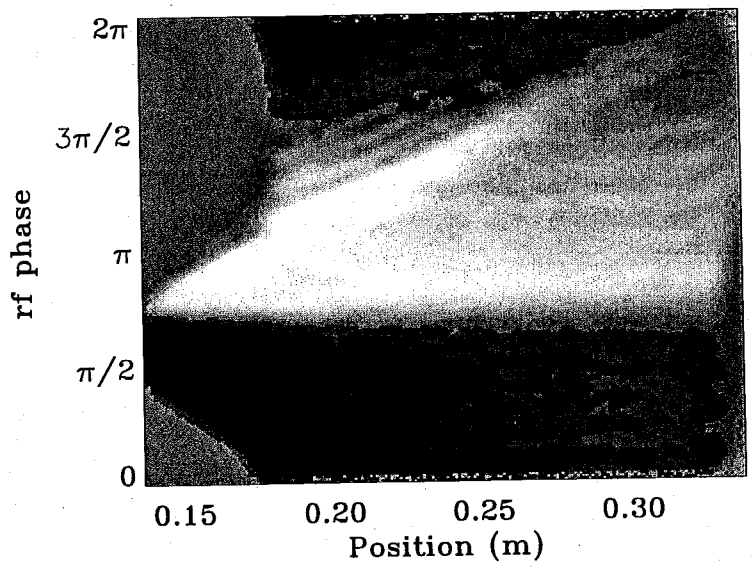

Figure 4.15 (a) 3d plot of the electron current as a function of phase and position, for $\alpha = 6$

(b) Image plot of the electron current. Current moving toward the live electrode is shown in black, zero current is orange, and current moving toward the grounded electrode is white.

and the sheath is moving most rapidly. The production of multiple beams occurs due to rotation of the electrons in phase space, as they are trapped in the large amplitude plasma wave created by the electron beam-plasma interaction. This effect has also been observed in a planar simulation of an rf plasma (Vender (1990)). The high energy electrons, which can escape the potential well, move across the plasma with an essentially constant velocity, producing the enhanced ionisation noted in Figure 4.14. The electron beams decrease in magnitude with at increasing phase but are still observable until approximately $\omega t = 3\pi/2$. Note that the sheaths are clearly delineated in this graph as regions of zero current.

Figure 4.15 (b) shows the same conditions plotted as an image, with colour used to indicate the direction and magnitude of the current. Positive current is represented by increasing darkness, negative by white and zero current is orange. This clearly emphasises the abrupt change in the current direction across the whole plasma as soon as the live sheath motion reverses direction. It also clearly shows the longitudinal waves in the current, and the directed electron beams originating from the sheath edge. Note also that at $\omega t = 3\pi/2$, when the sheath starts to collapse again the bulk electrons start moving back toward the live electrode (shown as the black region at the top of 4.15 (b)), but that the high energy electrons are still moving toward the grounded electrode.

Most of the electrons in the bulk have a temperature of about 3 eV – the density of the high energy electrons, created by interaction with the moving sheath edge, is around two orders of magnitude lower than the bulk density. As discused previously, in the bulk region the rf current is carried almost entirely by the electrons, and it is of interest to determine the relative fraction of the rf current carried by the high energy "beam" and low-energy bulk electrons. Figure 4.16 is a plot of the time-averaged electron current as a function of position in the plasma, showing the currents carried by high (> 3eV) and low energy electrons and the total current. This shows that almost *all* the rf current is carried by the small number of high energy electrons. In fact the low and high energy electrons can move in opposite directions, depending on position in the plasma and the phase of the cycle. On average the low energy electrons are moving toward the grounded electrode, while the high energy group is moving toward the live electrode. This indicates that the high energy group of electrons depends only on conditions at the live sheath, and the rf current is therefore expected to be relatively insensitive to the bulk electric fields.

This is further illustrated in Figure 4.17, which shows (a) the electric field and (b) the electron current as a function of position at various phases of the rf cycle. At $\omega t = 0$, $\pi/4$ and $3\pi/2$ the electrons are moving in the direction of the field and are therefore heated, while at $\omega t > \pi/2$ the current is in opposition to the electric field, leading to electron cooling. This is discussed further in Section 4.4.2

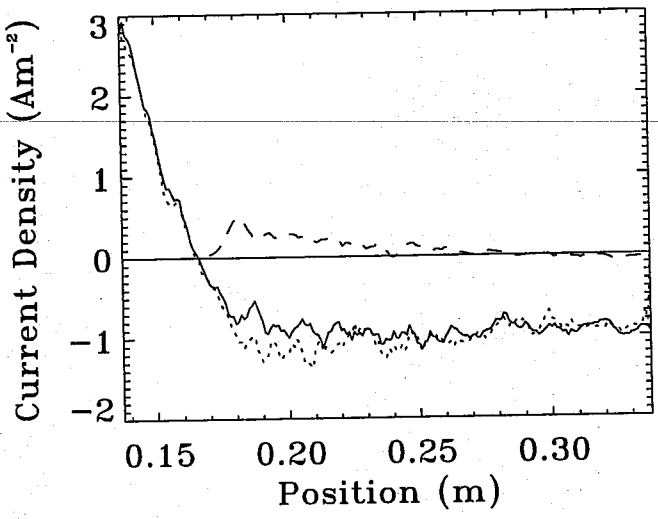

Figure 4.16 Time-averaged electron current density in the plasma, showing the total current (solid line), and the relative magnitudes carried by the high energy (> 3 eV) (dotted line) and low energy electrons (dashed line).

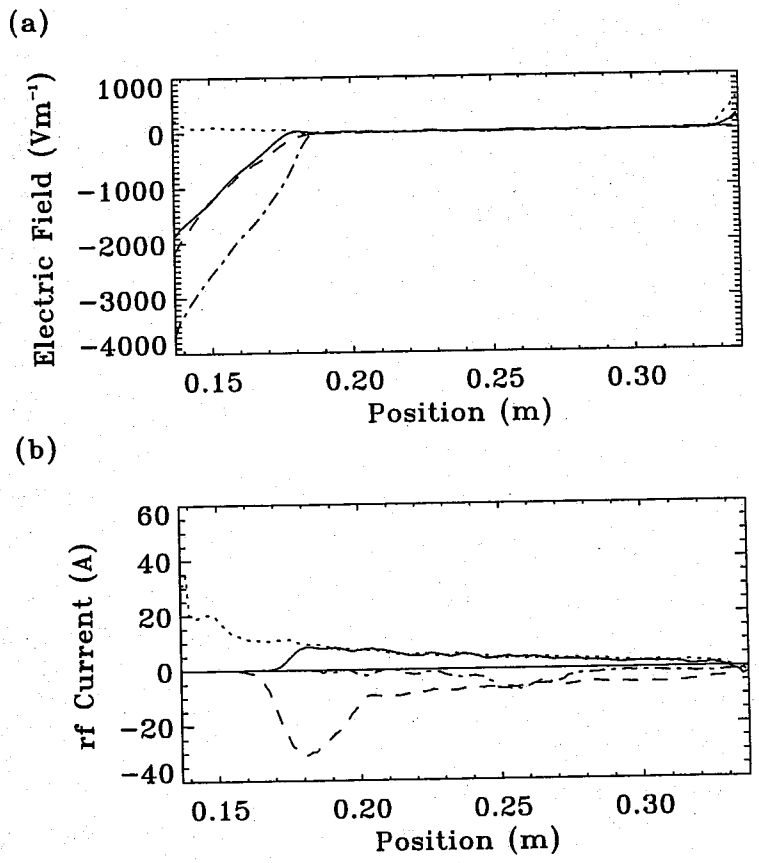

Figure 4.17 Plots of **(a)** electric field **(b)** total electron current as a function of position, shown at various phases of the rf cycle: $\omega t = 0$ (solid line), $\pi/4$ (dotted line), $\pi/2$ (dashed line), $3\pi/2$ (dash-dot line).

4.4 Power Absorption

The power absorbed by the plasma is an important parameter, since it determines the steady-state density of the plasma. The average power requirement over the rf cycle is determined by the loss rates for the ions and electrons, i.e., average power supplied by the generator = power lost to plasma by particle processes. Section 4.4.1 treats the average power loss in the cycle, while Section 4.4.2 and 4.4.3 deals with the individual loss rates due to the electrons and ions respectively.

4.4.1 Total Power Loss

The instantaneous power supplied to the plasma by the rf generator is given by

$$P(t) = V_{rf} \sin(\omega t)\, I_{rf}(t) \qquad (4.18)$$

where $I_{rf}(t)$ is the instantaneous current across the plasma. To first order the plasma current can be considered sinusoidal with the form $I_{rf}\sin(\omega t + \phi)$ where ϕ is the phase difference between the current and the voltage. The instantaneous power therefore has a period of twice the applied voltage, since $\phi \sim 90°$ due to the capacitive nature of the plasma.

Due to inertia the ions do not respond strongly to the instantaneous rf fields, therefore most of the instantaneous power transferred from the generator to the plasma goes into the redistribution of electrons between the sheaths as they expand and collapse. Since the rf current in the bulk is carried mainly by the electrons this simply represents the current flow through the system. This does not result in a change in the average electron energy, it merely imposes a drift velocity on the bulk distribution with no net transfer of power from the generator to the electrons. The net amount of power that has to be supplied by the source to maintain the plasma is determined by averaging over the rf cycle, and so the average total power, P_{tot}, can be determined by integrating (4.18)

$$\overline{P} = \frac{V_{rf} I_{rf}}{2\pi} \int_0^{2\pi} \sin(\omega t) \sin(\omega t + \phi)\, \mathrm{d}(\omega t)$$
$$= \frac{1}{2} V_{rf}\, I_{rf} \cos\phi. \qquad (4.19)$$

The phase difference, ϕ, is found to be approximately constant over the range of parameters used in the simulations and equal to ~73°. Hence equation (4.19) can be written simply as $P_{tot} = 0.151\, V_{rf} I_{rf}$. Results from the simulation (for all parameters) are

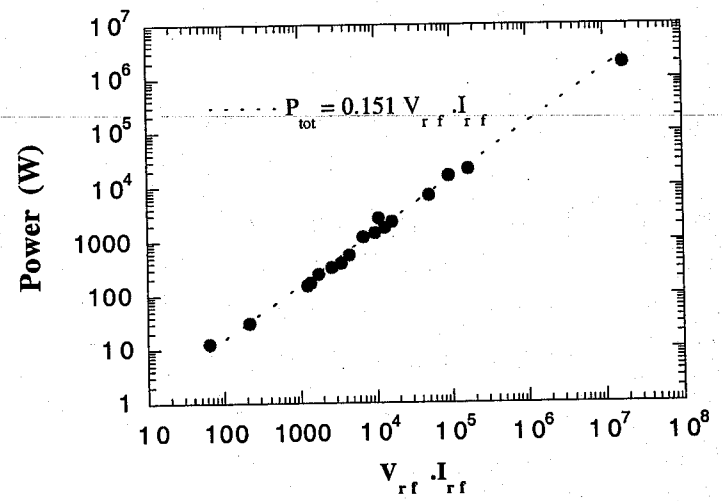

Figure 4.18 Average plasma power as a function of $V_{rf}.I_{rf}$, showing simulation results and the fitting from equation (4.19) (solid line)

plotted in Figure 4.18, and agreement with (4.19) is found to be extremely good over a range of seven orders of magnitude.

For a system at steady state the average power supplied to the plasma represents the energy required per cycle to balance loses through inelastic processes, and to maintain the density by balancing particle creation rates with the loss rates to the walls. Ions gain energy from the plasma through acceleration in the sheaths and this energy is consequently lost to the plasma when the ions reach the electrodes - in experimental systems the energy is dissipated as heat, secondary electron emission and sputtering, but in the simulation the walls are assumed to be perfectly absorbing. Electrons gain energy in the bulk through momentum transfer collisions with the neutrals in a process known as ohmic heating, and through interactions with the oscillating sheath edge in what is called stochastic or sheath heating (see Section 4.4.2). Electrons lose energy through inelastic collisions (ie ionisation and excitation collisions) and to the walls when the sheath collapses.

Many authors (including, but not exclusively, Koenig and Maissel (1970); Keller and Pennebaker (1987); Horwitz (1983); Bletzinger and Flemming (1987); Godyak, Piejak and Alexandrovich (1991b); Wood, Lieberman and Lichtenberg (1991)) have designed equivalent circuit models of rf plasmas in order to predict parameters such as the plasma density, ion currents to the electrodes, the sheath behaviour and the dependence of the sheath voltage ratio on the electrode area ratio. In order to design a useful model the electrical characteristics of low pressure plasma need to be well understood. Typically the sheath and bulk regions are modelled using separated sub-circuits. Following

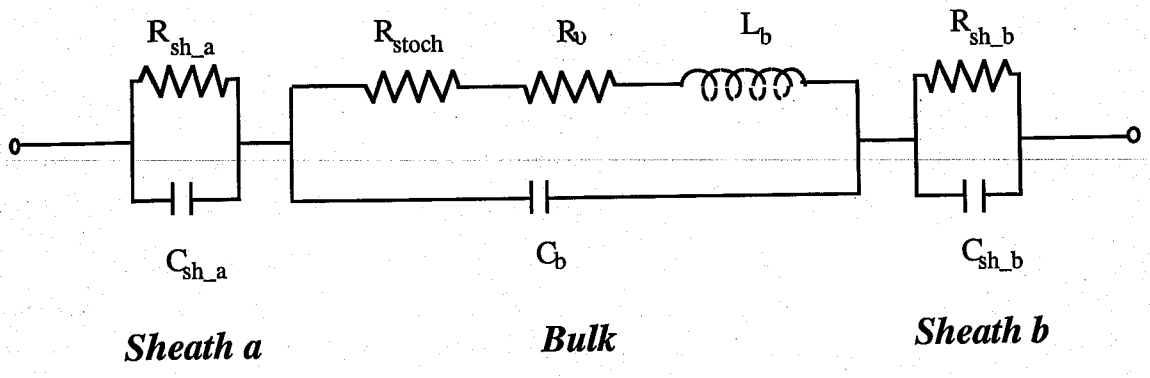

Figure 4.19 Equivalent circuit model of an asymmetric plasma, separating the components into the bulk and the two sheath regions.

Godyak's model, shown in Figure 4.19, the bulk is assumed to have two resistive components, R_υ, corresponding to ohmic heating, and R_{st} to stochastic heating. These resistors are in series with an inductor, L_b, which represents the inertia of the electrons in the rf field; and in parallel with a capacitor, Cb, which represents the amount of displacement current in the bulk. For most conditions in weakly ionised rf plasmas electrons in the bulk effectively react instantaneously to the fields, which means that L_b can be ignored. The displacement current in the bulk can also be assumed to be negligibly small compared to the conduction current, so the bulk capacitance is infinite and C_b can also be neglected. Note that this final assumption breaks down at high pressures and very small discharge currents – for these conditions the plasma permittivity approaches 1, which can result in significant penetration of the rf field into the plasma bulk, and hence the assumption of a negligible displacement current is no longer true. According to Godyak *et al* C_b becomes significant for pressures of 1 Torr and currents of less than 0.01A, and at increasing current for higher pressures. Since the simulation is limited to pressures of less than 0.5 Torr, it is assumed that L_b and C_b can safely be ignored. Hence the series resistance of the plasma is simply given by $R_p = R_{st} + R_\upsilon$.

Each sheath is modelled using a capacitor, C_{sh}, in series with a resistor, R_{sh}. Note that in the symmetric system, the sheaths are equivalent so they can be conveniently modelled by a single capacitor and resistor, but in the asymmetric system the sheaths must be modelled individually. However, for large area ratios most of the power dissipation in the plasma occurs at the live sheath and under certain conditions it can be sufficient to model that sheath only. Section 4.4.2 gives a detailed analysis of the electron energy gain and loss mechanisms in the plasma, and compares simulation results to theories developed by Godyak *et al* (1991b) and Misium *et al.*(1989). In Section 4.4.3 the ion energy gain in the sheath is determined and related to the sheath resistivity, again comparing theory and simulation.

4.4.2 *Energy balance for the electrons*

Since the bulk discharge current is carried mainly by the electrons most of the instantaneous power goes into transporting the electrons between the sheaths. However the process is not perfectly elastic and energy is dissipated by the electrons through ionisation and excitation collisions, and when the electrons escape to the walls. The average power during the rf cycle supplied to the electrons must therefore balance these energy losses in order to maintain steady-state conditions. There are two primary mechanisms by which electrons are heated in rf discharges with negligible secondary emission (Surrendra and Graves (1991)):

(1) electrons in the vicinity of the sheath region are heated by the oscillating sheath fields.

(2) electrons in the man body of the plasma are heated by the bulk fields which drive the rf current.

The first method is generally known as sheath (or stochastic) heating and the second as bulk or ohmic heating.

As mentioned in the previous section, the rf current in the bulk of the plasma is carried mainly by the electrons. The fields which drive the current can therefore heat the electrons, provided that the electron motion is in phase with the local electric field – this is ohmic heating. Ohmic heating is known to be particularly effective in heating the electrons when the oscillating fields in the bulk are relatively small, i.e., when the applied voltage is low or the gas pressure is high (Godyak *et al* (1991b), Surrendra and Graves (1991)). An equation describing ohmic heating P_ν in planar geometry is given by Missium *et al* (1989). This equation has been modified to take into account the spherical geometry giving

$$P_\upsilon = \frac{1}{2}\int_{r_{sa}}^{r_{sb}} \frac{m\upsilon\, I_{rf}^{\,2}}{e^2 n(z)\, 4\pi (r_a + z)^2}\, dz, \qquad (4.20)$$

where υ is the electron-neutral collision frequency and is assumed to be constant across the plasma (i.e., electrons are assumed to have a constant, well-defined temperature), and r_{sa} and r_{sb} are the radii of the live and ground sheath edges respectively. Godyak *et al* (1991b) and Surrendra and Graves (1991) derive a similar equations to Misium *et al* but use the average plasma density instead of integrating. For the simulation parameters results for both methods are very close for most conditions. Using the area at the centre of the plasma and the average density instead of integrating over r works very well except at large area ratios (e.g., $\alpha > 15$). Results from equation (4.20) and the simulation are plotted in Figure 4.23, together with sheath heating results.

Sheath heating results from the interaction of electrons with the oscillating sheath-plasma boundary. In the 1950s it was observed that ionisation is enhanced at the sheath edges, from which it was assumed that the motion of the sheath must somehow be involved in heating the electrons. According to Goedde *et al* (1988) the underlying mechanism for heating is Fermi acceleration, in which the electrons can gain energy through reflection from the moving sheath when the correct plasma conditions exist. In determining whether Fermi acceleration will heat the electrons it is necessary to consider transport through the bulk plasma as well as the sheath properties. At extremely low pressures (<< 1 mTorr) the electrons make no collisions when traversing the bulk and so their motion becomes correlated with the sheath motion, and no energy is transferred. At intermediate pressures (1 – 100s of mTorr) collisions randomise the phase with which electrons arrive at the sheath, so that energy can be exchanged between particle and field. At higher pressures the electron mean free path becomes very small, so the moving sheath can impart little energy to the electrons – in this case ohmic heating dominates.

Goedde *et al* (1988), Godyak *et al* (1991), and Misium *et al* (1989) have determined models of sheath heating which treat the sheath edge as a step-like profile with which the electrons make hard-wall collisions. From conservation of momentum an electron hitting the "wall" with a velocity v_o will be reflected with a velocity of $2v_w + v_o$, where v_w is the sheath-edge velocity. When the sheath is expanding into the plasma electrons moving toward the electrode will be reflected with increased energy; and when the sheath is collapsing the electrons will lose energy. Using this model the authors mentioned above have determined equations for the power gained by the electrons through sheath heating.

Again the equation for the planar system is taken from Misium *et al* and modified for the spherical system. (Godyak *et al* derive a similar equation, but Misium *et al* include an extra term to take into account for non-uniform ion density in the sheath, and the time-varying electron density). In spherical geometry the power gained by sheath heating is given by

$$P_{sh\_o} = 0.336 \frac{m\langle v_e \rangle}{e^2} \left(\frac{s_o}{\lambda_D} \right)^{2/3} \frac{I_{rf}^{\,2}}{n_{so} A_{so}}, \qquad (4.21)$$

where the subscript $o = a$ at the live sheath and b at the grounded sheath, $\langle v_e \rangle$ is the electron thermal velocity, n_s is the density at the sheath edge, and A_s the area at the maximum sheath expansion. In the asymmetric system the heating should be calculated separately at each electrode, although for large area ratios essentially all of the electron heating occurs in the vicinity of the live sheath (see Figure 4.21), so the grounded sheath can be ignored. Experimental detection of stochastic heating in an argon plasma has been inferred from measurements of the plasma resistance (Bletzinger and Flemming (1987)).

To determine the rate of transfer of energy into the electrons, measurements of the electron power can be determined from the simulation from the product of the electron current density and the field at each grid point $J.E$. Figure 4.20 (a) shows a 3-D graph of the power deposition into the electrons as a function of position and phase for $\alpha = 1$. Positive values of the power indicate electron heating, while negative values indicate cooling. Figure 4.17 (b) is an image plot overlayed with contour lines of the same conditions; the darkness of the image indicating increasing power deposition. Figure 4.21 shows the same plots for $\alpha = 6$. Figure 4.20 clearly shows that the power deposition is heavily dependent on phase and position. Heating occurs predominantly at the moving sheath edge – most of the heating occurs during the expansion phase of the sheath (i.e., for $\pi/2 < \omega t < \pi$ at the live electrode), but some heating can also be seen when the sheath is collapsing ($0 < \omega t < \pi/2$). This is contrary to the expectation of the hard-wall model, which predicts that the electrons should lose energy during the contraction phase, but concurs with experimental measurements of the electron energy in a low pressure nitrogen plasma (Turner and Hopkins (1992)). There is also a brief period close to the live electrode at $\omega t \sim \pi/2$ (and correspondingly at $\omega t \sim 3\pi/2$ close to the grounded electrode) for which power deposition becomes negative. This can be seen in Figure 4.20 (b) in the white dot at ~100°. This represents the electron cooling which occurs when electrons are moving in opposition to the local electric fields. It occurs at the beginning of the expansion phase of the sheath since electrons are still diffusing toward the electrode due to inertia, even after the fields in the sheath have reversed. As noted in Section 4.2.2 the electron density in the sheath is still substantial for this phase, even when the sheath potential is several hundred volts negative (see Figure 4.12). In other words there is a phase-lag between the sheath expansion and the reversal of the electron velocity distribution which is obviously not representative of a hard-wall interaction. It can be seen from this plot that ohmic heating, which occurs mainly in the bulk where the densities are high, is small compared to sheath heating. Similar forms for the electron power deposition have been found in planar models of rf discharges (Graves (1987), Sommerer, *et al* (1989b), Surrendra and Graves (1991)).

A comparison of Figures 4.20 and 4.21, shows that at $\alpha = 1$ the power deposition is very symmetric with equal peaks at each electrode, but for the higher area ratio case power deposition occurs almost entirely at the live sheath edge. The live sheath increases and the grounded sheath decreases with increasing area ratio, resulting in a much larger live sheath velocity and therefore a higher rate of energy transfer to the electrons. For $\alpha > 1$ most of the heating takes place at the live electrode, and the grounded sheath can be ignored. For $\alpha = 6$ the power transferred to the electrons peaks much higher at the live electrode than the symmetric case due to the increased sheath velocity, but the total power transferred to the electrons has decreased. Note in Figure 4.21 (a) beams of energetic electrons can be seen streaming out from the expanding

(a)

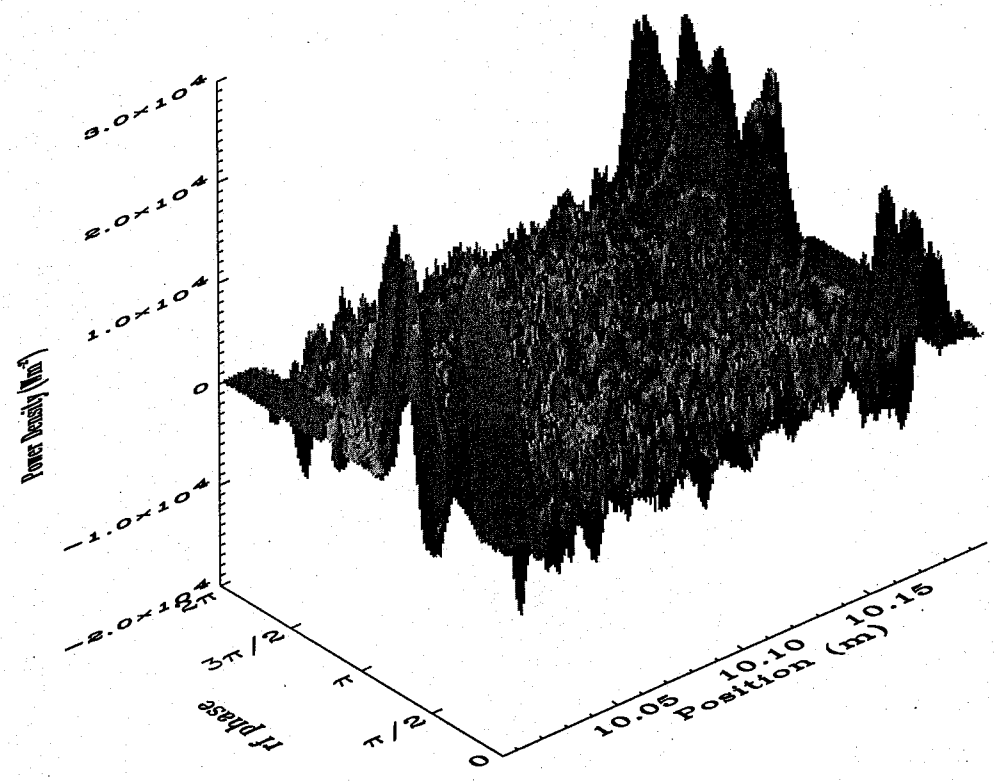

(b)

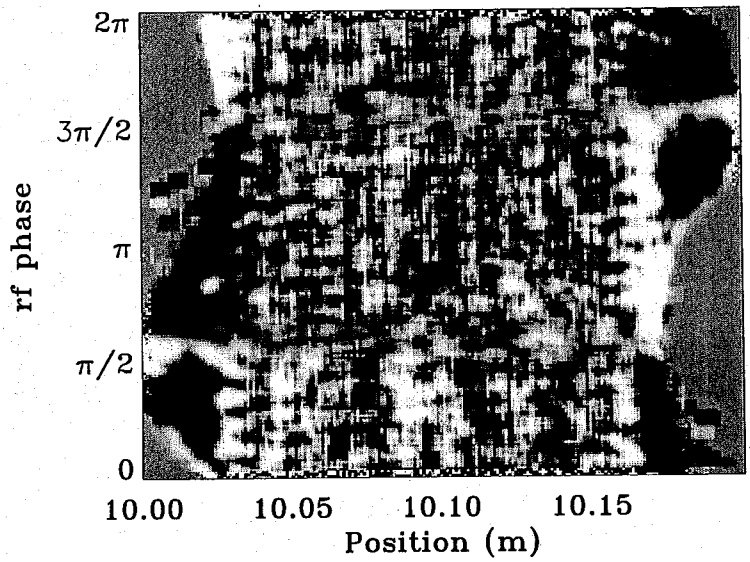

Figure 4.20 (a) 3d plot of power deposition into the electrons as a function of phase and position for α = 1

(b) Image plot of the power deposition. Regions of positive power deposition are dark, the background orange represents zero and regions of power loss are white.

(a)

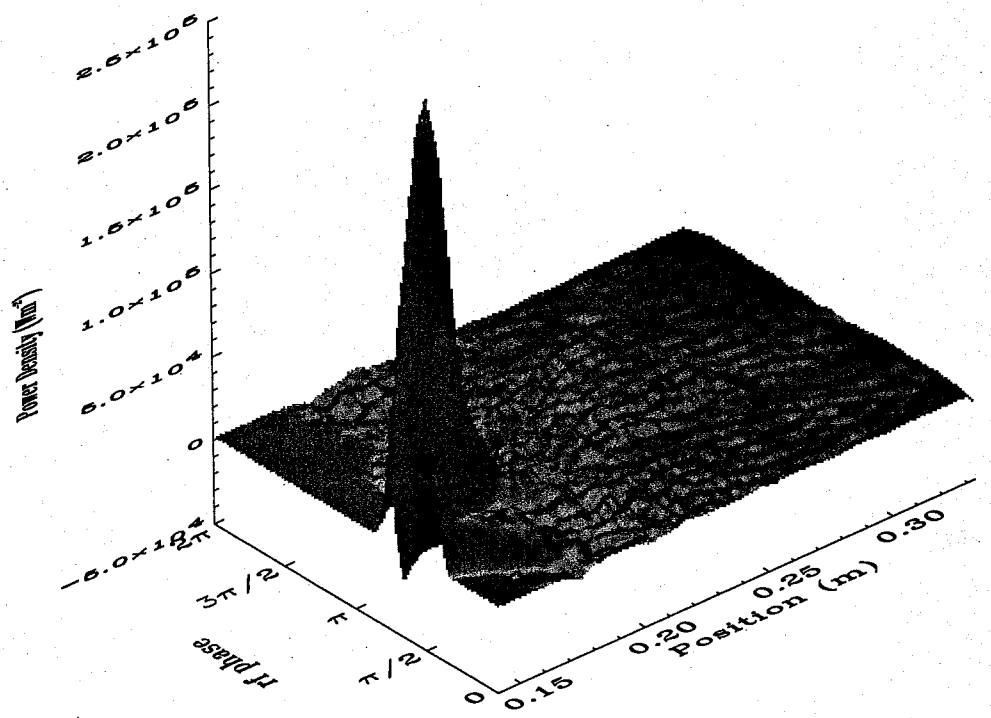

(b)

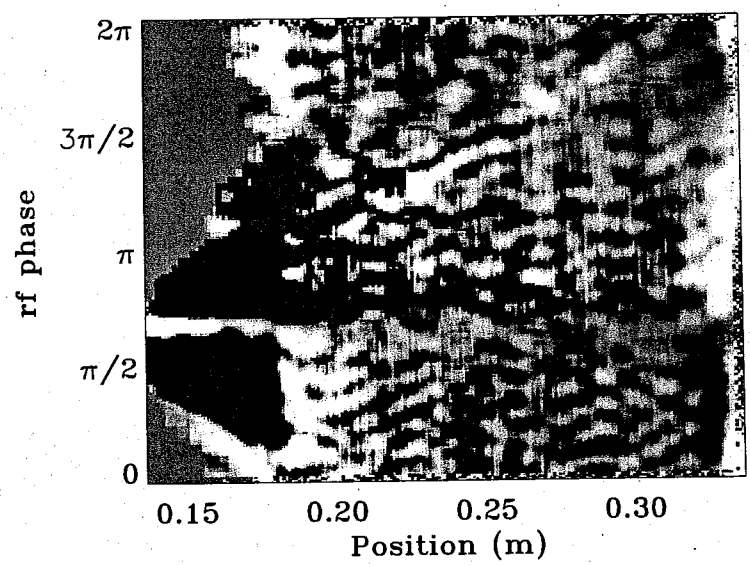

Figure 4.21 (a) 3d plot of power deposition into the electrons as a function of phase and position for α = 6

(b) Image plot of the power deposition. Regions of positive power deposition are dark, the background orange represents zero and regions of power loss are white.

sheath edge, these can also be seen in the 3-D current plot, Figure 4.15, for the same conditions. Electrons in these beams often have energies in the order of tens to hundreds of electron volts and can be tracked by regions of higher ionisation. Energetic electrons which traverse the interelectrode gap without making a collision can then escape to the grounded electrode or be reflected from the sheath, depending on energy and arrival time.

Figure 4.22 shows the time-averaged power as a function of position for various area ratios . The sheath heating is delineated by the position of the maximum sheath edge, so that as area ratio increases the peak in the sheath heating broadens, due to the corresponding increase in sheath width. The height of the peak decreases at increasing area ratio, since the total power decreases with increasing area ratio due to a corresponding drop in plasma density. Note that the power deposition at the grounded electrode is negative on average, due to electrons diffusing against the local fields at this position. At the live electrode the effect of cooling is negligible compared to heating.

Integrating simulation values for the electron power separately for the sheath and the bulk regions, a rough determination of ohmic and sheath heating can be determined. This method is only approximate, since it differentiates between heating mechanisms only by position, assuming that power changes in the bulk are entirely due to ohmic heating, and in sheath region to sheath heating. Results thus derived from the simulation are plotted in comparison to results from equations (4.20) and (4.21) in Figure 4.23 as a function of area ratio; and the sum of the (4.20) and (4.21) is compared to the sum of the

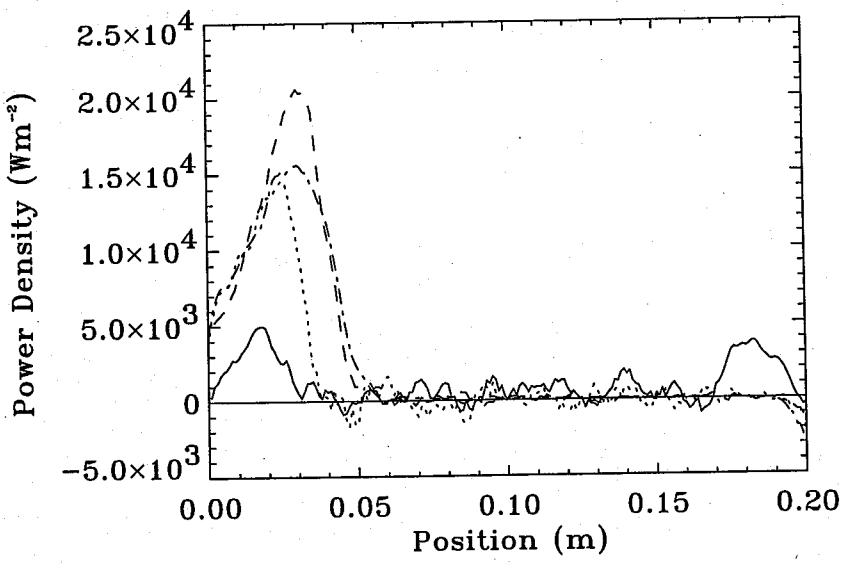

Figure 4.22 Time-averaged electron power as a function of position shown for area ratios: $\alpha = 1$ (solid line), $\alpha = 2$ (dotted line), $\alpha = 6$ (dashed line) and $\alpha = 15$ (dash-dot line)

simulation values (which is just equal to the total electron power). For small area ratios the agreement between simulation and calculated values is fairly good, and the total powers compare well. However at increasing area ratio the correspondence becomes increasingly worse – simulation results for ohmic heating are much less than the calculated values, and for sheath heating are much smaller than predicted. This indicates that modifying the planar equations for a spherical system does not adequately represent the physics at large area ratios. Note that for area ratios 2 and 4 the simulation indicates that on average there is electron *cooling* in the bulk (the power is therefore negative and do not appear on the plot). That is electrons appear to be losing energy though ohmic heating rather than gaining it.

Results in planar PIC simulations (Surrendra (1991)) also find lower rates of ohmic heating than those calculated from the planar version of equation (4.20). This can be related to transport of the rf current in the bulk. In Section 4.3 it was found that the rf current is carried predominantly by high energy (>3 eV) electrons, which are decoupled from small variations in the bulk electric fields, and that at certain phases the rf current moves in opposition to the bulk fields. The electrons carrying the current will therefore lose energy at these times, and under certain conditions this could lead to a net cooling effect in the bulk.

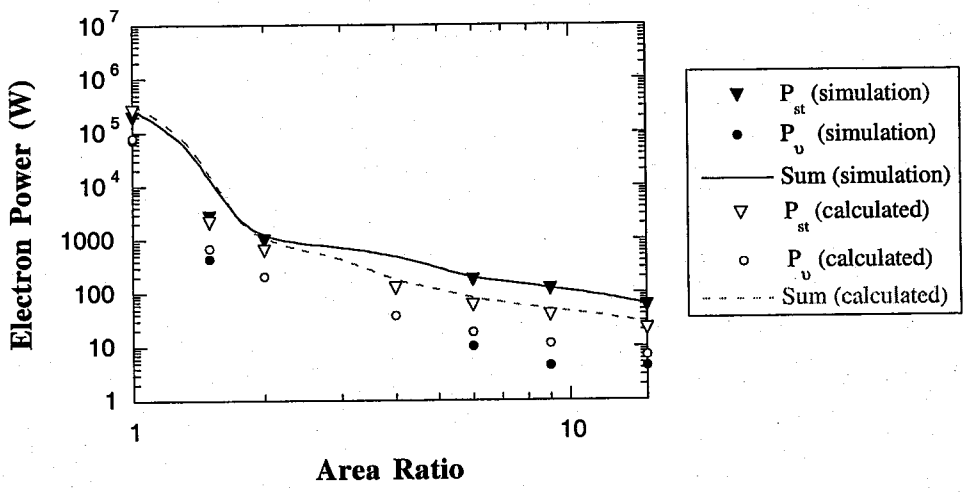

Figure 4.23 Power deposition into the electrons from P_{υ} (dots) and P_{sh} (triangles) calculated using equations (4.20) and (4.21) plotted in comparison to simulation results. The sum of the calculated results are also compared to the total electron power from the simulation.

For sheath heating the difference between simulation and calculation is difficult to determine – possibly equation (4.21) needs to be re-derived specifically for the spherical geometry, since simplifying assumptions used for planar systems do not apply in the asymmetric case. It is also possible that the hard-wall model of the sheath is simply not a good representation of the electron-sheath dynamics – as previously mentioned in this section there are results which suggest that this model is not applicable, particularly for the case of field reversal in the sheath resulting in beam-like electron energy distributions. This effect occurs particularly at high area ratios, where agreement between simulation and theory is worst.

As a further test of the simulation results the energy lost through collisions with neutrals and the walls can be compared to the total power deposited into the electrons. At steady-state the losses and gains would be expected to balance when averaged over a cycle. Walls are assumed to be perfectly absorbing so the energy lost by colliding electrons can be calculated by integrating over the energy distribution at the electrode. This is approximately equal to the product of the average flux ,Γ, and the average energy of the escaping electrons, ε (in eV). The average electron flux over one cycle must be equal to the average ion flux, so the electron power loss to each wall can further be simplified to the product of the ion current and the average electron energy at the electrode

$$P_{wall} = \frac{m\omega_{rf}}{4\pi}\left[\frac{\int_0^\infty v^2 f(v)dv}{\int_0^\infty f(v)dv}\right]_{a+b} = e(\Gamma_a A_a \varepsilon_a + \Gamma_b A_b \varepsilon_b) = i_a \varepsilon_a + i_b \varepsilon_b \qquad (4.22)$$

The energy lost through ionisation and excitation collisions can be determined by integrating the collision rate per electron over the whole population of electrons. This integral is simplified by assuming that the collision frequency is constant for all electrons (i.e., electrons are assumed to have a constant temperature, independent of position or phase) and that only ionisation and excitation collisions result in an energy loss (equal to the threshold energy for the interaction)

$$P_{coll} = e(\upsilon_{ion}\varepsilon_{ion} + \upsilon_{exc}\varepsilon_{exc})\int_{r_{sa}}^{r_{sb}} n(z)4\pi z^2\, dz. \qquad (4.23)$$

Note that this equation only includes collisions in the bulk. Assuming that the cross-sections for excitation and ionisation have roughly the same form, as is the case for hydrogen, then the excitation rate can be written as a multiple of the ionisation rate – $\upsilon_{exc} = n\upsilon_{ion}$, where n depends on the average electron temperature. From equation (3.51) $4\pi e\int \nu_I z^2 n(z)dz$ is equal to the ion current, so (4.23) can be written as

$$P_{coll} = (\varepsilon_{ion} + n\varepsilon_{exc})(i_a + i_b). \qquad (4.24)$$

For an average electron temperature of 3 – 4 eV in atomic hydrogen $n \approx 3.3$. Equations (4.23) and (4.24) are solved for different area ratios using simulation values for the average electron energies and the ion currents, and the results plotted in Figure 4.24. The sum of the losses is compared to the total electron power transferred to the electrons. The results show very good agreement between simulation and the sum of equations (4.20) and (4.22), although at high area ratios the total loss rates are slightly smaller than the energy transferred to the electrons. The relative proportion of energy lost through collisions drops compared to loss rates to the walls at higher area ratios, probably due to the assumption of constant collision frequency in deriving (4.21). Results from Chapter 3, show that in fact the average bulk temperatures are not independent of position, particularly at large area ratios. Furthermore using an average temperature to determine collision rates does not take into account the high energy tail of the electron energy distribution, which will have disproportionately higher collision rates, and this tail increases at large area ratios due to the electron-sheath dynamics.

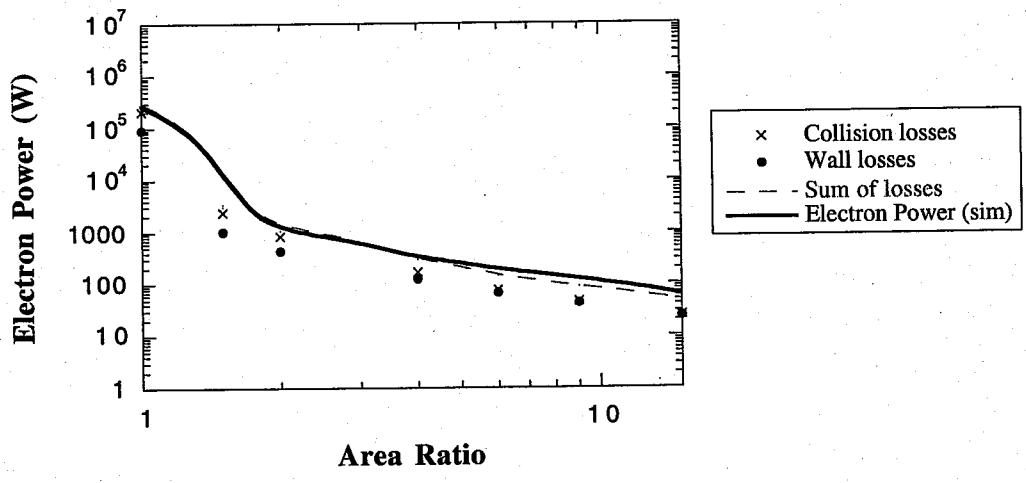

Figure 4.24 Electron power losses P_{wall} and P_{coll} calculated from (4.22) and (4.24), and their sum (dashed line) compared with the total electron power gain (solid line) as a function of area ratio.

4.4.3 *Ion Energy Balance*

Power is transferred from the plasma to the ions as they are accelerated through the sheaths by the time-averaged electric field, and is consequently lost when the ions hit the electrodes. The ion power loss can therefore be easily calculated by integrating over the ion energy distribution at the electrodes for one cycle. An average value can also be determined from the product of the ion current at the electrode and the average sheath potential, although this is more approximate since it does not take into account the spread in the ion velocity distribution due the rf voltage oscillation.

$$P_{ion} = \frac{M_{ion}}{4\pi e}\omega_{rf}\left[\frac{\int_0^\infty u^2 f(u)\,\partial u}{\int_0^\infty f(u)\,\partial u}\right]_{a+b}, \qquad (4.25)(a)$$

$$= i_a V_a + i_b V_b. \qquad (4.25)(b)$$

Comparing results from both methods of calculation gives essentially the same results. Only when the transit time of the ion through the sheath is much shorter than the rf period will there be any noticeable discrepancy between the two values (the effect of sheath transit time on the ion energy distribution is discussed in Section 4.6.1). Note that in the symmetric system the currents and voltages at each sheath are equal, but for asymmetric simulations $i_a V_a >> i_b V_b$. Therefore in the symmetric system ($\alpha = 1$) the total ion power is $P_{ion} = 2 i_a V_a$; while for $\alpha > 1$ it can be approximated by $P_{ion} = i_a V_a$. In effect the grounded sheath contributes negligibly to the total power, this has also been noted for stochastic heating in the electrons.

Although the sheath impedance is considered to be dominantly capacitive, there must also be a resistive component to account for power transfer to the ions as they are accelerated through the sheath. The power dissipated by ions falling through the sheath can therefore be related to the sheath resistance, since the capacitive impedance effects only the electrons. From Godyak *et al* (1991a) the power deposited into the ions is related to the sheath impedance by

$$P_{ion} = \frac{1}{2} I_{rf} R_{sh}^{\ 2} \qquad (4.26)$$

Godyak *et al* (1991a) also give an equation determining the sheath resistance of a symmetric system as a function of the sheath voltage and width and the ion current. Re-writing this for a spherical coordinate system, the following expression is determined

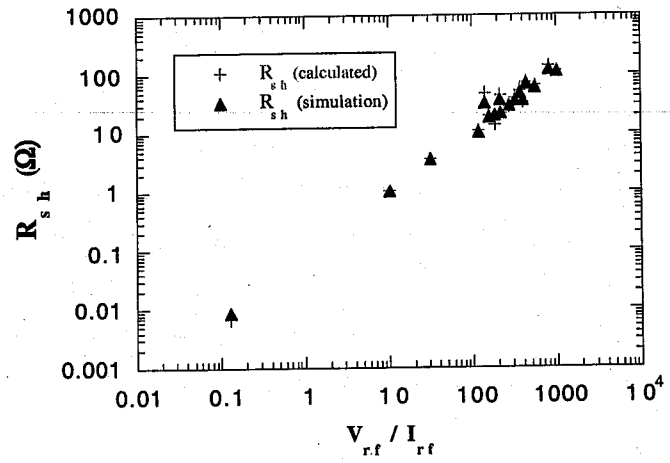

Figure 4.25 Comparison of calculated and simulation values for the total sheath resistance

$$R_{sh\_o} = \frac{1}{16\,\varepsilon_o^{\,2}\pi^5 f_{rf}} \frac{i_o V_o}{|V_o|^2} \left(\frac{s_o}{r_o}\right)^2 (r_o \pm s_o)^{-2} \qquad (4.27)$$

where $o = a$ for live sheath quantities and b for the grounded sheath. The resistances calculated from equation (4.27) are plotted as a function of V_{rf}/I_{rf} and compared to simulation results determined using equations (4.25) and (4.26). The results are plotted in Figure 4.25 and are found to have remarkably agreement for the whole range of parameters.

Finally to determine the relative power deposition into ions and electrons, the fractions P_{ion}/P_{tot} and P_{elec}/P_{tot} are plotted in Figure 4.26. This clearly shows that at low input powers approximately half the total power goes into each of the ions and electrons, but at higher values the ions gain a much larger fraction than the electrons. The reason for this can be seen using quite simple arguments. Taking equations (4.22) and (4.24) for the electron power losses, and assuming that the ion currents to the live and grounded electrodes are approximately equal (true to within a factor of ~ 2), then for $\alpha > 1$ $P_{elec} = i_a\left(2\varepsilon_{ion} + 2n\varepsilon_{exc} + \varepsilon_a\right)$, where ε_{ion} = 13.6 eV, ε_{exc} = 10.2 eV and the average energy of electrons escaping to the wall ε_a is approximately 100 eV (the value at α = 15). This gives a rough value for the electron losses of $P_{elec} \approx 200\, i_a$. The total power depends on the applied voltage, and from (4.25) so also will the ion power loss through the average live sheath potential. The minimum total power will therefore be at V_{rf} = 100 V, for which $P_{ion} \approx 90\, i_a$, and the maximum at V_{rf} = 5 kV, when $P_{ion} \approx 4400 i_a$. So from this rough argument the ion power will vary from roughly half the electron power at

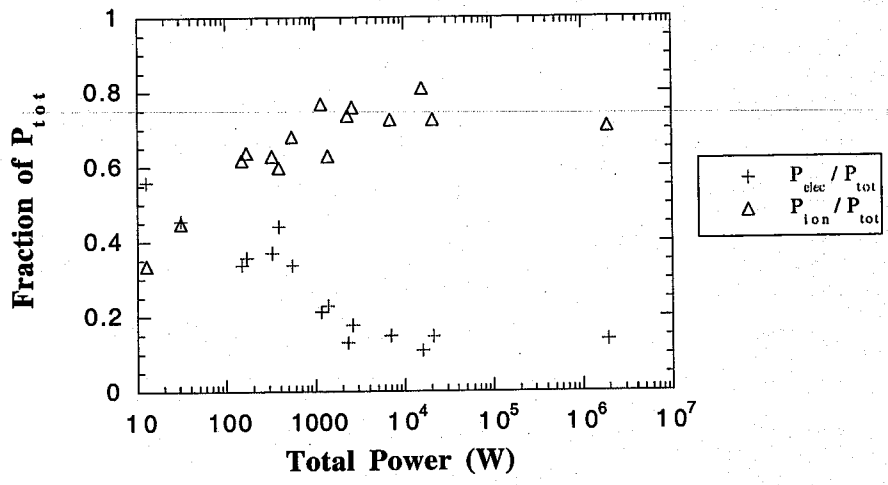

Figure 4.26 The relative values of ion and electron powers plotted as a function of the total power.

low total powers, to approximately 20 times larger at high powers. In fact, from Figure 4.26, the electron power drops to only about 1/10 of the ion power at large total powers. This is because energy losses to the wall also increase with increasing applied voltage due to field reversal effects, but the flavour of the argument still holds, since the difference between electrode and plasma potential will never be larger than the average potential across the sheath.

In summary, both electron and ion heating occur almost entirely at the live sheath in low-pressure asymmetric systems. The calculated electrons losses concur well with the heating determined from the simulation, but the calculated stochastic and ohmic heating values are too low. The sheath resistance calculated from the ion power loss, matches well to theoretical values for the whole parameter range. Power is shared almost equally between ions and electrons at low input powers, but at high powers almost 80% goes into the ions.

4.5 Comparison between collisionless and collisional ion simulations

Most of the results presented in this thesis so far have concentrated on the collisionless ion model. However for experimental conditions at these pressures the mean free path is on the order of millimetres and so ions would be expected to undergo many

collisions, particularly in the bulk. It would therefore be instructive to have a comparison between collisional and collisionless simulation parameters in order to identify the effects due to collisions. Table 4.1 presents a comparison between a number of different parameters for $\alpha = 6, V_{rf} = 1$ kV, $p = 20$ mTorr and $f_{rf} = 10$ MHz. From the table it can be seen that the biggest variation occur in the plasma density, with the peak density increasing by nearly an order of magnitude; in the average kinetic energy of the ions which decreases by the same amount and in the ion current to the grounded electrode which decreases by 50%. The average power dissipated and the average sheath voltages are almost unchanged by the inclusion of collisions. The ion currents decrease with the introduction of collisions, while the total rf current increases.

The large increase in density occurs due to the reduced ion mobility in the bulk – ions can only move a few millimetres before making a collision and therefore gain little energy from the small bulk fields. This sharply increases the time taken to diffuse from the centre of the plasma to the ion sheath edge, and so reduces the loss rates considerably. Reduced loss rates lead to a drop in the creation rate required to sustain steady-state conditions, hence the reduction in the average electron energy – the ionisation rate similarly shows a decrease of ~ 40%. Evidence for a reduced ion mobility can also be seen in Figure 4.27 which plots the parallel velocity phase space for (a) collisionless (b) collisional ions. Figure 4.27 (a) clearly shows that the pre-sheath fields extend all the way through the plasma, and the ions have well-defined drift velocities throughout the bulk. In 4.27 (b) ion velocities are much more thermalised, and the pre-sheath extends only a few millimeters – approximately the distance between collisions – from the edge of the ion sheath. The points at which ions are accelerated in the sheaths are clearly discernible in the collisionless case and the sheath velocities are well defined, while for collisional ions the sheath edges are less well-defined and there is a spread of velocities in the sheath due to collisions. Charge exchange collisions in the sheath reduce the average kinetic energy of the ions – charge exchange is a process in which an ion exchanges energy with a neutral, resulting in a low (~1/40 eV) energy ion and a fast neutral. The charge exchange mean free path is much smaller than the sheath width, so there is a high probability of ions making at least one charge exchange collision in the sheath. This causes the large drop in the average ion energy.

From the data in Table 4.1, the power and live sheath voltage for both collisional and collisionless ions are very similar, so from the previous section the ion flux to the live electrode must also be equivalent. The density increases by an order of magnitude for collisional ions and so for a constant flux the ion velocity must decrease by the same. However, this would appear to result in a violation of Bohm's law at the sheath edge, since to maintain a positive potential in the sheath the velocity of ions entering the sheath must be at least equal to the ion sound speed. To determine if this violation does occur it

	Collisionless Ions	Collisional Ions	% difference
n_{peak} (m^{-3})	4.5×10^{14}	2.6×10^{15}	+ 580 %
P_{avg} (W)	556	550	- 1 %
i_a (A)	0.42	0.36	- 14 %
i_b (A)	0.76	0.31	- 59 %
I_{rf}	4.46	6.12	+37%
V_a (V)	880	910	+3%
V_b (V)	38	44	+15%
V_{bias}	-842	-856	+2%
s_a (m)	0.048	0.031	- 35 %
s_b (m)	0.009	0.008	-10 %
kTe_{ion} (eV)	3.5	0.31	- 91 %
kTe_{elec} (eV)	5.5	3.4	- 38 %

Table 4.1 Comparison of plasma parameters between collisionless and collisional ion simulations for $\alpha = 6$, $V_{rf} = 1$ kV, $p = 20$ mTorr and $f_{rf} = 10$ MHz.

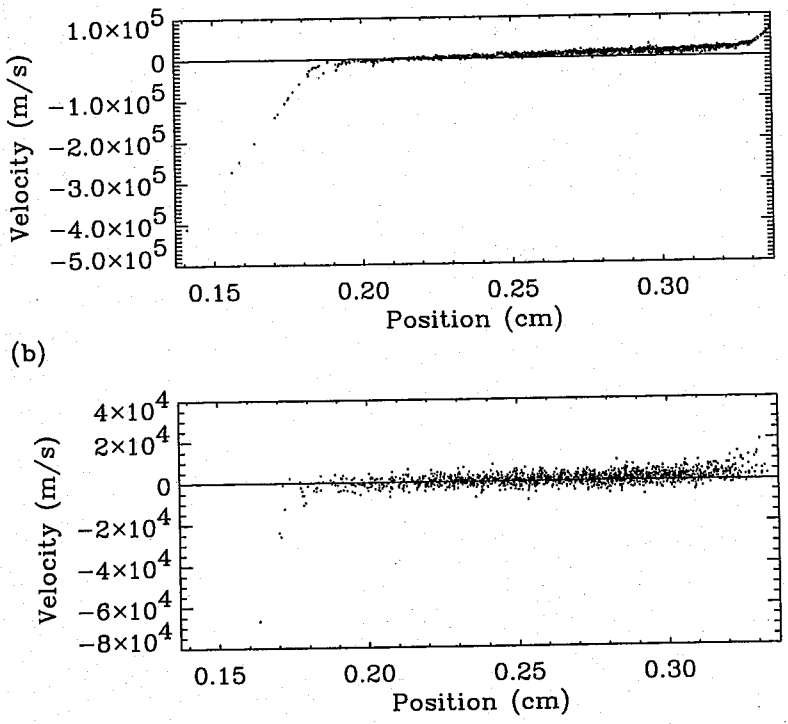

Figure 4.27 Ion parallel velocity phase plot for **(a)** collisionless ions **(b)** ion-neutral collisions. Conditions are $\alpha = 6$, $V_{rf} = 1$ kV and $p = 20$ mTorr.

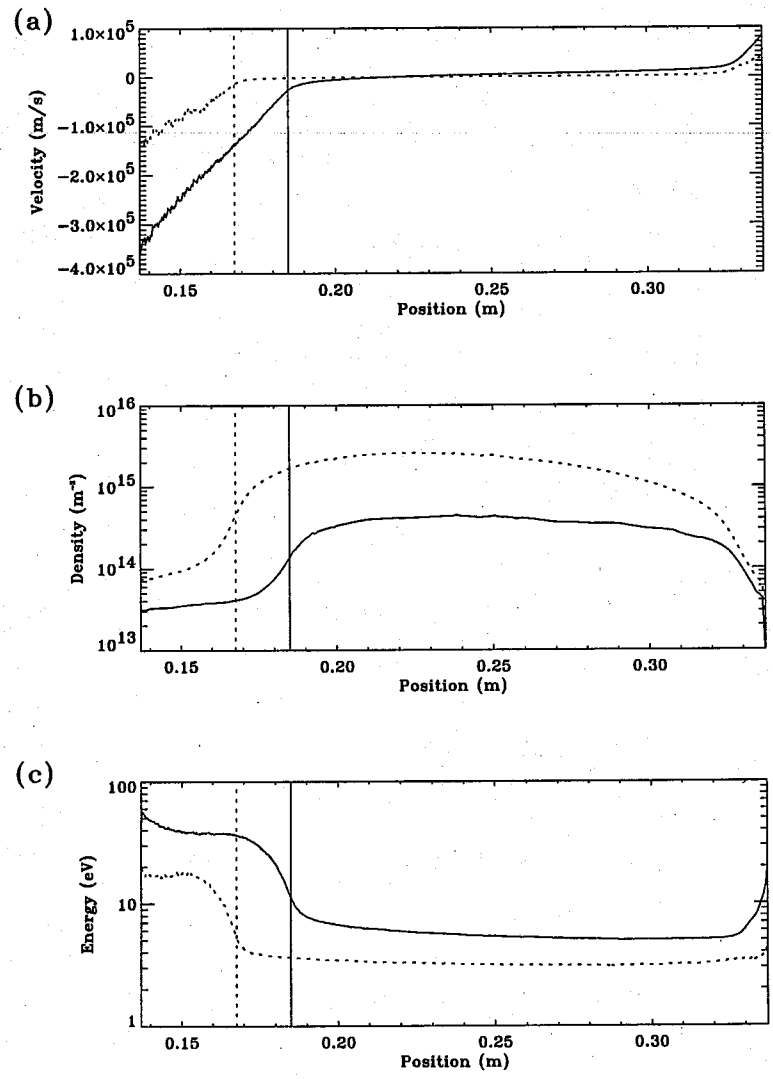

Figure 4.28 Average values of **(a)** ion velocity **(b)** ion density **(c)** electron energy plotted as a function of position. Results are shown for both collisionless (solid line) and collisional (dotted line) ions. The vertical lines show the respective positions of the ion sheath width.

is necessary to have a closer look at the ion flux close to the sheath edge. Plotted in Figure 4.28 as a function of position are (a) the average ion velocity (b) the ion density (c) the average electron energy, for both collisional and collisionless ion cases. From (c) the average electron energy close to the ion sheath width for the collisionless ion case is about 7 eV. Assuming that the temperature can be related to the average energy by $kT_e = 2/3\varepsilon$ then $kT_e = 4.7$ eV, giving an ion sound speed of $u_S = 2.6\text{x}10^4$ ms^{-1}, which

corresponds exactly to the average velocity at the sheath edge in Figure 4.27 (a). From Figure 4.28 (b) the density at the sheath edge is 1.5×10^{14} m^{-3}, giving a flux of Γ=4.2x10m^{-2}s^{-1}.

For the collisional ions, from Figure 4.28 (c) kT_e = 2.7 eV, giving an ion sound speed of $u_S = 1.6 \times 10^4$ ms^{-1} (so roughly 2/3 of the collisionless ion sound speed). Again this corresponds well to the average velocity in Figure 4.28 (a) of 1.8×10^4 ms^{-1}, so obviously Bohm's criterion is obeyed in the collisional case. The density at the sheath edge from (b) is approximately 7×10^{14} m^{-3}, giving a flux of $\Gamma = 11 \times 10^{18}$ m^{-2}s^{-1}, so in fact the collisional flux is about 3 times that of the collisionless at the sheath edge. However, due to the reduced ion mobility in the sheath, the average collisional ion velocity at the electrode is only 1/3 of the collisionless ion velocity, and although density at the electrode is still higher the relative fluxes for the collisionless and collisional cases are $\Gamma_{nc} = 11 \times 10^{18}$ m^{-2}s^{-1} and $\Gamma_c = 13 \times 10^{18}$ m^{-2}s^{-1} respectively. Hence Bohm's criterion is preserved in the case of ion collisions and the fluxes at the electrodes are approximately equal for both collisionless and collisional ions, as expected from the results in Table 4.1.

4.6 Ion distribution functions at the electrodes

For systems in which ion collisions can be neglected the average ion energy at the surfaces can be easily determined from the average sheath potentials. For asymmetric systems the sheath potential at the live electrode is the sum of a dc bias voltage and the plasma potential, while that at the grounded sheath is simply the average plasma potential (see Section 4.1.2). In very asymmetric systems the bias voltage is very large and the plasma potential very small, making the bias voltage a good measure of the average live sheath potential. The ion energy distribution can also be substantially broadened by rf effects, depending on the length of time the ion spends in the sheath compared to the period of the rf cycle, so to fully characterise the ion energy distributions at the electrode surfaces it is important to know the amplitude of the sheath voltage and the maximum sheath width, as well as the average potential.

For systems in which ion collisions are important – and this includes most of the pressure range used in RIE – collisions play a substantial role in determining the energy distributions. Ions will typically make many collisions in the bulk, but have little directed energy due to the low fields in the bulk, so energies remain essentially thermal. In the sheath, however, ions are accelerated by the field and gain substantial energy parallel to the field direction. This energy can then be transferred into angular momentum through elastic collisions with neutrals, resulting in broadening of the angular distribution at the

electrode. Charge exchange collisions in the sheath will substantially lower the average energy of ions arriving at the substrate, and also produce highly energetic neutrals which can effect the substrate surface. To determine energy and angular distributions at surfaces in the reactor it is therefore important to model these collision processes.

Ion energy distributions are examined for various plasma conditions in the following sections.

4.6.1 Collisionless ions

The phase of the rf cycle at which the ion enters the sheath determines the potential across the sheath at the time of entry, and therefore the initial acceleration of the ion. If the ion spends many rf cycles traversing the sheath this information will be lost and the ion will arrive at the electrode with the average sheath potential. If, however, the time taken to transit the sheath is of the same order as the rf period, then the entry conditions will be important in determining the final velocity and ions will not all reach the substrate with the average energy. In this case the IEDF will have more structure than would occur in a dc system. Figure 4.29 and Figure 4.30 show the ion energy distributions with area ratio, and pressure as parameters respectively. The double-peaked distribution is typical of rf systems, since the sheath potential varies sinusoidally with time (see Figure 4.2) and so more time is spent at values close to the minimum and maximum voltages. The distribution therefore peaks at the extremes and a local minimum at the average potential, which the sheath sweeps through rapidly. The EDF is symmetric about the average energy, so that the peaks are equidistant from the centre. IEDFs have been intensively studied for rf discharges and this distribution has been experimentally verified for collisionless ions by many authors (see Coburn and Kay (1972), Kuyper and Hopman (1988), Greene *et al* (1988), Wild and Koidl (1991), Flender and Wiesemann (1994))

Figure 4.29 (a) is a plot of the live IEDF as a function of area ratio, this shows that the average ion energy increases with area ratio as expected, since the average sheath potential is known to increase with α (see Figure 4.6). The average ion energy from the IEDF is defined to be the energy mid-way between the two peak energies, rather than the true average of all ion energies at the electrode, comparison between the average ion energy and the average sheath potential is presented in Figure 4.31. The energy separation of the peaks also increases with area ratio – this quantity depends on the sheath potential and width, and results from an analytic expression is compared to the simulation later in this section. The energy peaks show some asymmetry – for example distributions at the live electrode have larger peaks on the high energy side. According to

(a)

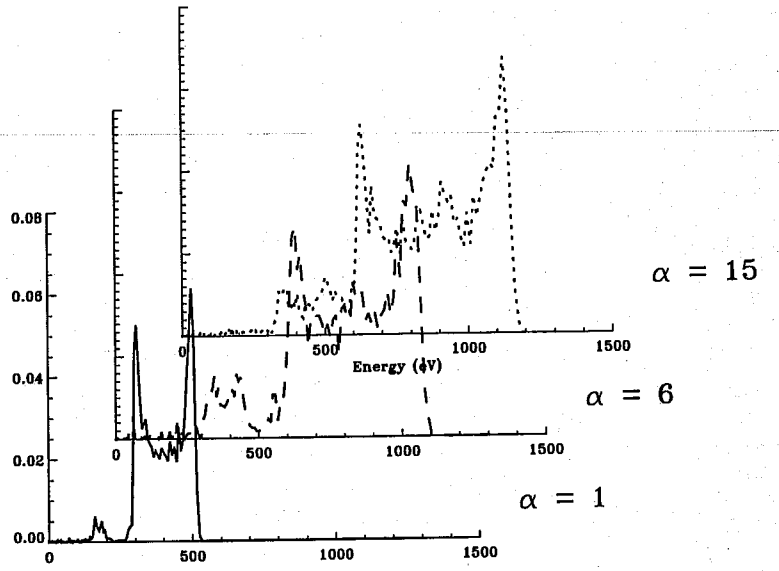

(b)

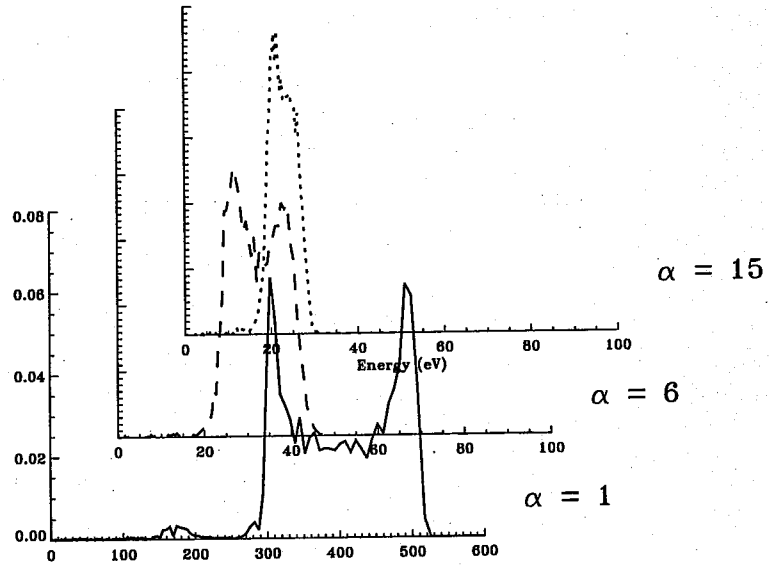

Figure 4.29 Ion energy distribution of collisionless ions as a function of area ratio at **(a)** live electrode **(b)** grounded electrode.

Field *et al* (1991) this is typical of distributions of light ions; although simulation results at the grounded electrode have a higher low energy peak which would appear to contradict this explanation. Another point to note from Figure 4.29 (a) are the small features at low energy, which also appear to show a double-peaked distribution. These are due to ionisation in the sheath region during the period of the sheath collapse, resulting in the creation of very low energy ions in the middle of the sheath which are then swept up by the advancing sheath edge. The effect is more noticeable at higher area ratios, since more energetic electrons are produced.

(a)

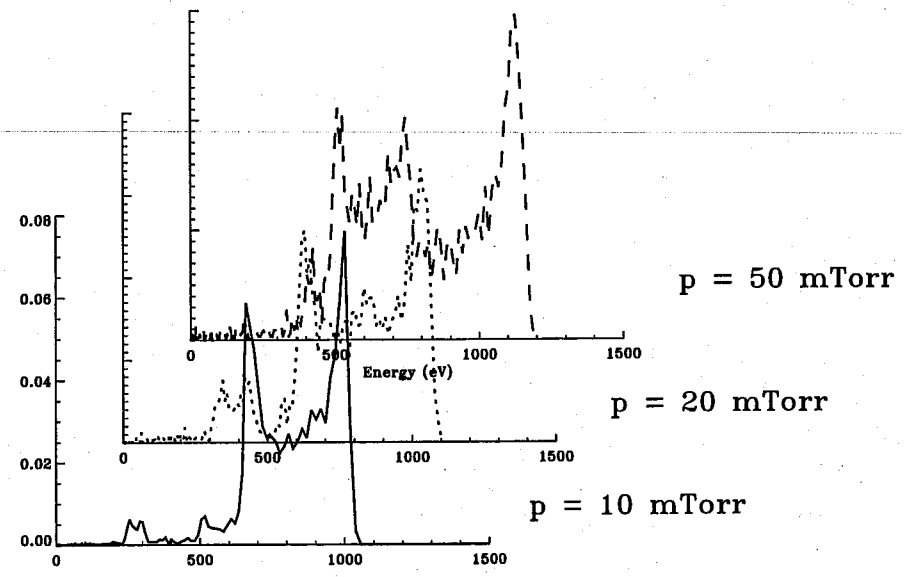

(b)

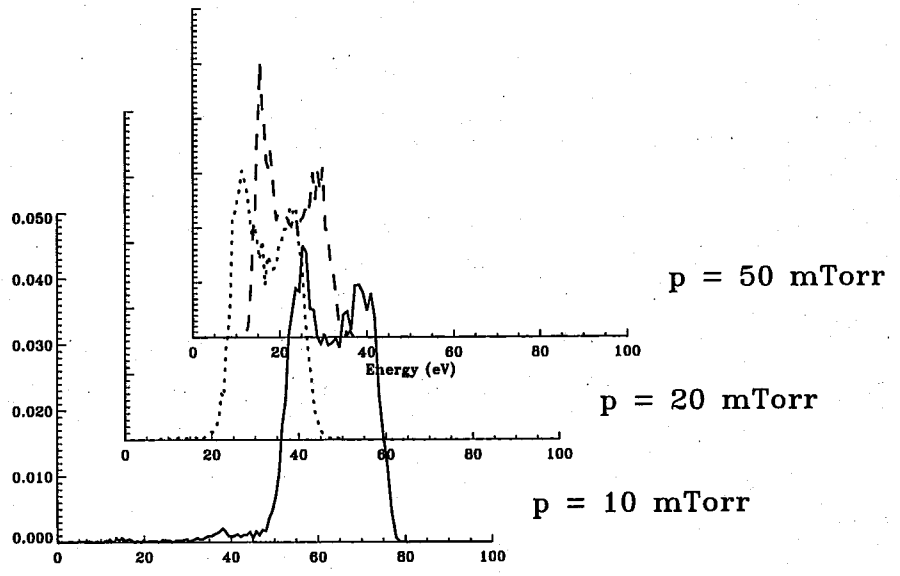

Figure 4.30 Ion energy distribution of collisionless ions as a function of pressure at **(a)** live electrode **(b)** grounded electrode.

For the grounded electrode, Figure 4.29 (b), it can be seen that the energy distribution moves to lower average energies as the average grounded sheath potential decreases, and that the peak separation also decreases, until at $\alpha = 15$ there is only a single peak. A single peaked structure indicates that the ions are spending many rf cycles in the sheath until their energy is entirely averaged and independent of the entry phase.

Figure 4.30 (a) shows the IEDF at the live electrode for a range of pressures. There are a few differences from Figure 4.29 to note, namely that at higher pressures more structure can be seen in the distributions, and at $p = 50$ mTorr the IEDF has three peaks rather than two. This is again due to ionisation in the sheath by energetic electrons

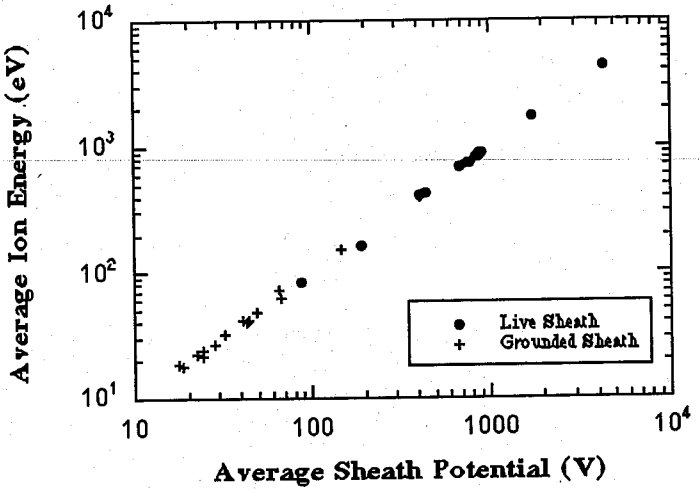

Figure 4.31 Average ion energy determined from the mid-position of the two peaks in the IEDF, plotted as a function of the average sheath potential for live (dots) and grounded (crosses) sheaths.

– at higher pressures the ionisation rate is large enough to produce a substantial numbers of low energy ions in the sheath, resulting in a distribution function which can interact with that of ions entering the sheath from the bulk.

Figure 4.31 is a plot of the average ion energy (i.e., the energy mid-way between the peaks) plotted as a function of the average sheath potential for all simulation parameters. Agreement between the two parameters is extremely good for the whole range of parameters for both live and grounded sheaths. Hence IEDFs of collisionless ions can be used to determine the average sheath potential in experimental set-ups, where it can be difficult to make measurements of the bulk potential. This would only work for a limited range of conditions (i.e., at low pressures, when ions can be considered collisionless) and since most processing reactors have complex chemistries, with many different charged molecules present, the IEDFs can be difficult to interpret.

Various authors have determined analytic expression for the energy separation of the peaks in the rf ion energy distribution, however the derivations typically have the same form and differ only by a constant factor. Using the expression from Manenschijn *et al* (1991)

$$\Delta E = \frac{2ne|V|}{\omega s}\sqrt{\frac{2q\overline{V}}{m_i}}, \qquad (4.30)$$

where q and m_i are the charge and mass of the ion, ω is the rf frequency, $|V|$ is the amplitude of the sheath voltage and $\overline{V}$ the average, and n is a constant which depends on

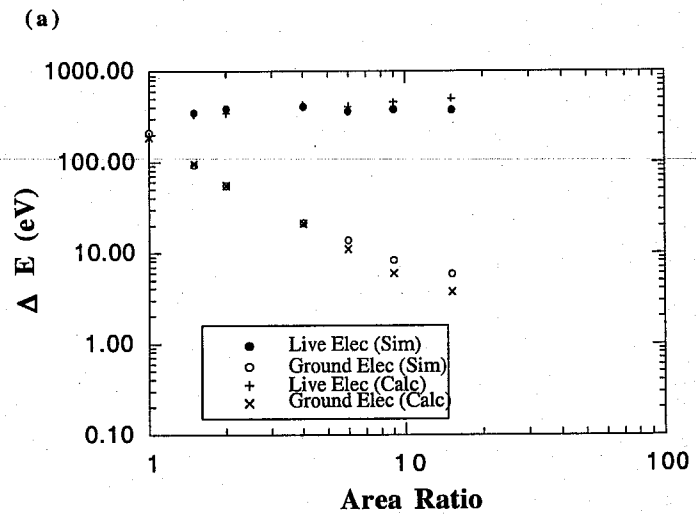

Figure 4.32 Energy separation of bimodal peaks in IEDF peaks as a function of area ratio. Simulation results are plotted in comparison to results from (4.30).

the collision dynamics. Manenschijn *et al* specify a value of $n = 4/3$, for collisionless ions. However in comparison to the simulation it was found that $n = 2/9$, gave a better fitting. The results from equation (4.30), with $n = 2/9$, are plotted as a function of area ratio in Figure 4.32 in comparison to simulation results. The results compare extremely well at low area ratios, but do show slight disparity at the higher area ratios. Simulation values for the live electrode are a little lower than those calculated from (4.30) while the reverse is true for the grounded electrode. This seems to indicate that equation (4.30) does not work as well for very asymmetric systems, possibly due to field reversal effects at the electrode mentioned previously in this chapter.

As mentioned previously, the form of the IEDF depends on the phase of the cycle that the ion enters the sheath, and on the length of time spent in the sheath. Wild and Koidl (1991) give an analytic expression for the collisionless ion transit time as a function of the sheath parameters:

$$\frac{\tau_{ion}}{T} = \frac{\omega s}{\pi}\sqrt{\frac{m}{2e\overline{V}}}, \qquad (4.31)$$

where τ_{ion} is the transit time across the sheath, and T the period of the rf cycle. The results from (4.31) are plotted in Figure 4.33 and indicate that the transit time for both live and grounded sheaths is approximately equal for all area ratios, despite the differences in sheath potential and width. This would appear to contradict the results for the IEDFs at high area ratios, which show large peak separations at the live electrode –

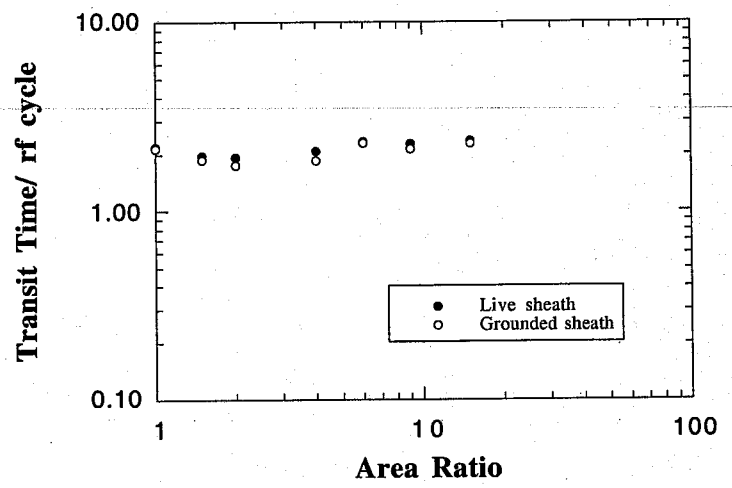

Figure 4.33 Ratio of ion transit time in the sheath to rf period plotted for live and grounded sheaths

indicating very little averaging of the ion energy, and therefore short transit times – and almost single-peaked distributions at the grounded electrode, indicating long transit times. Possibly the transit times cannot be so simply discerned from the peak separation, or perhaps equation (4.31) does not hold well for asymmetric systems. Simulation results are not generally available for ion transit times, so it is difficult to determine agreement between the simulation and equation (4.31), but some results for $\alpha = 6$ are discussed next.

To gain a better understanding of ion motion in the sheath, trajectories of a number of ions in the live sheath were determined for $\alpha = 6$. Ions were chosen randomly as they entered the sheath, and their total energy stored as a function of position until the electrode was reached. Results are plotted in Figure 4.34 for 9 ions. These plots indicate that ions enter the sheath with approximately the same energy (determined by the Bohm criterion) and on average spend 3 – 4 cycles in the sheath. The intermissions, when the sheath is collapsed, can be seen as periods of constant energy. In the first cycle the ions gain little energy, but by the third cycle they have reached substantial fractions of the sheath potential, and differences in the final energy are easily apparent. In essence ions can be considered as a mono-energetic beam on entering the sheath edge, with the structure in the energy distribution at the electrode due solely to the entry phase. Note that the average number of cycles spent in the sheath predicted by equation (4.31) is 2.2, which is slightly lower than the value estimated from Figure 4.34; although it must be noted that only a small number of ions were sampled, and that the estimation for the number of cycles depends very strongly on the position chosen for the sheath edge.

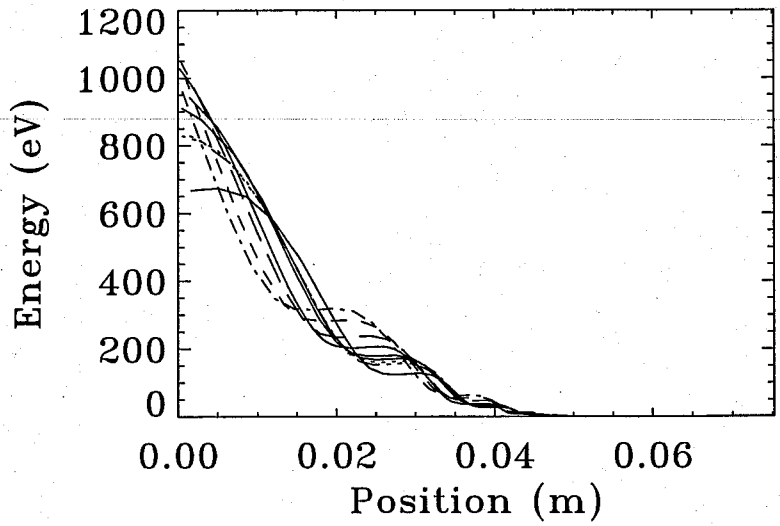

Figure 4.34 Collisionless ion trajectories in the live sheath for $\alpha = 6$, showing the total ion energy as a function of position. Flattening of the ion trajectories indicate periods of sheath collapse.

4.6.2 Collisional ions

The introduction of ion collisions to the simulation results in a substantial drop in the average ion energy, as is shown in Table 4.1. This can be directly attributed to the effect of charge exchange collisions on the IEDF in the sheath. For pressure in the 10 - 100 mTorr range the charge exchange mean-free pathlength is of the order of 8 - 2 mm, while the maximum sheath widths are approximately an order of magnitude larger. Most ions will therefore make many charge exchange collisions in the sheath before reaching the electrode, and each collision results in complete loss of the energy previously gained through acceleration by the sheath fields. Charge exchange therefore acts to cool the ion energy distribution at the electrode, and furthermore randomises the ion arrival time at the electrode with respect to the phase of entry to the sheath .

Elastic collisions, while having little effect on the total energy of the ions, determines the ratio of the energy distributed between the parallel and perpendicular direction, which results in broadened angular distributions at the electrodes producing detrimental conditions for etching. Transferring radially directed energy into angular momentum also results in the ions spending more time in the sheaths.

Figure 4.35 and 4.36 show the total ion energy for the same conditions given in Figure 4.29 and 4.30. Looking at Figure 4.35, the area ratio case, the IEDFs have completely changed from the distinctively bimodal peaks of the collisionless ion structure, instead they feature a much broader structure, with a large number of noisy

peaks, which extends across the whole energy range. The distributions now show a large number of ions at the low energy range, with only a very few reaching the electrode with the peak energy, indicating a substantial drop in the average energy of ions arriving at the electrode. From this it is expected that most of the ions have undergone at least one

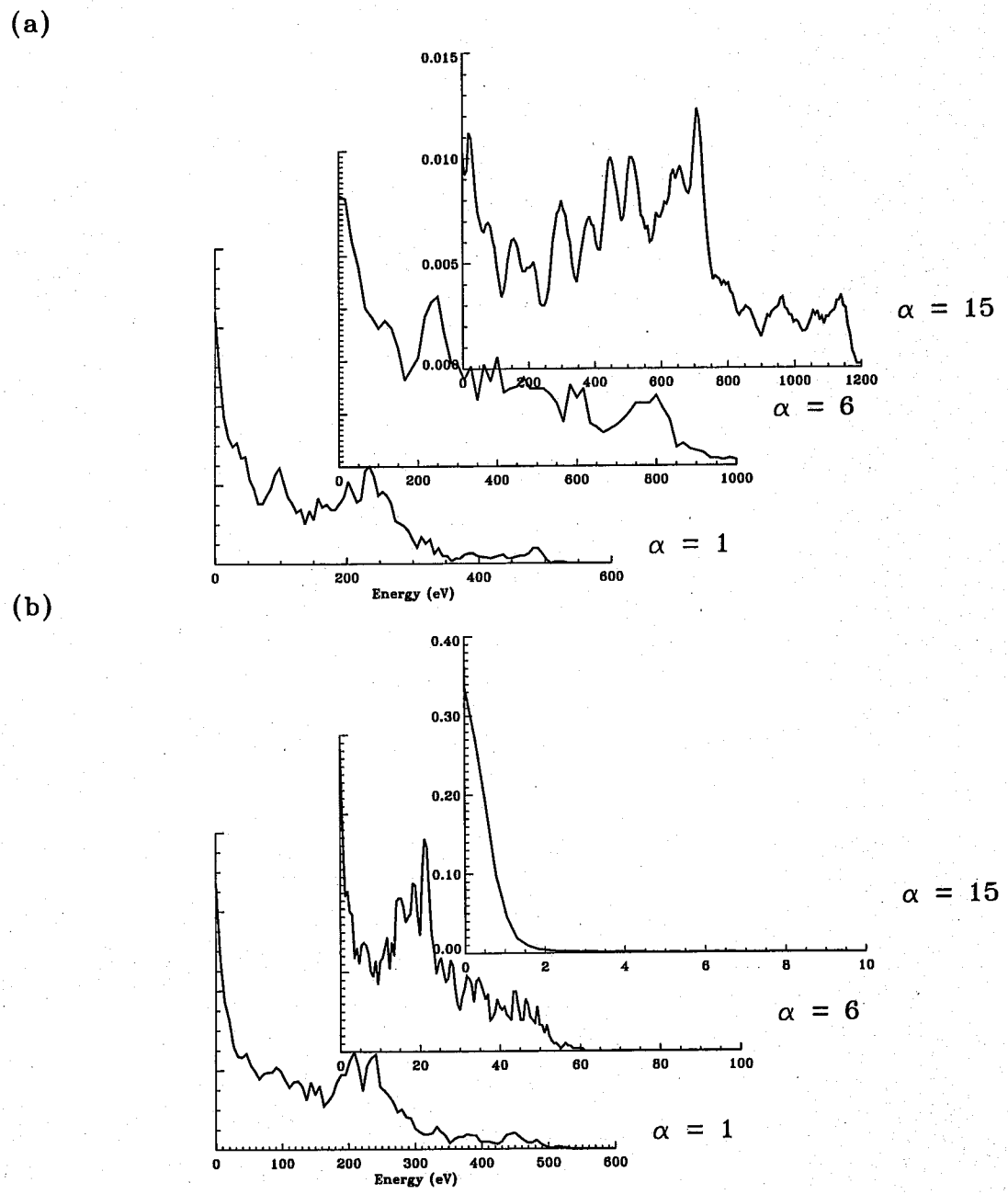

Figure 4.35 Ion energy distribution of collisional ions for different area ratios at **(a)** live electrode **(b)** grounded electrode.

charge exchange collision in the sheath, and in fact the ion mean free path for charge exchange at 20 mTorr is on the order of a few millimetres, indicating that ions would be expected to make several collisions in sheaths with widths of a few centimetres.

Figure 4.36 shows the variation with pressure emphasising the role of collisions

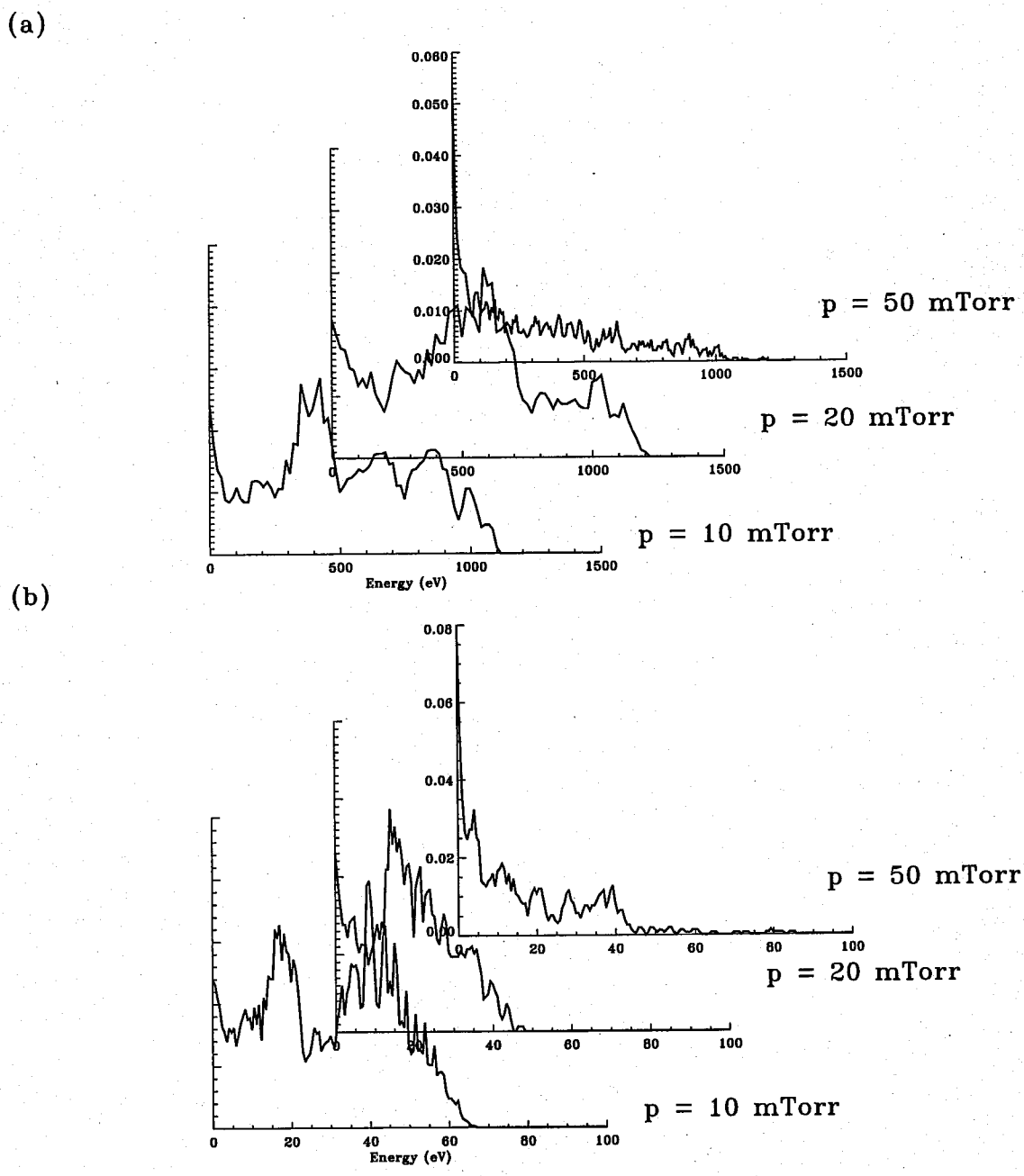

Figure 4.36 Ion energy distribution of collisional ions for different pressures at **(a)** live electrode **(b)** grounded electrode.

in determining the IEDF. At 10 mTorr quite a few ions still arrive at the electrode with the peak energy, indicating that these ions manage to cross the sheath without making a collision. As the background pressure is increased more collisions occur in the sheaths and the distribution moves to lower energies, until at 50 mTorr the distribution approaches an exponential form with a large peak close to zero energy, indicating a highly collisional sheath. Although the sheath width decreases with pressure, from a live sheath width of 5.7 cm at 10 mTorr to 2.8 cm at 50 mTorr , the mean free path for charge exchange decreases at the same time from 6 mm to 1.2 mm. Therefore the ratio of sheath width to mean free paths/λ increases from 9.5 to 23.3 over the pressure range.

Wild and Koidl (1991) have modelled the effects of charge exchange in the sheath on the IEDF. Their distributions show pronounced structure of peaks, which occur when the local electric field approaches zero at the moment a stationary ion is created by a charge exchange collision. The distributions found from the simulation also exhibit a peaked structure, but the peaks are broader and have more internal structure. This could be due to elastic collisions (which Wild and Koidl ignore) effectively smearing out the charge exchange peaks. Or it could be connected to other approximations in the theory, such as using a linear electric field in the sheath, or assuming that the charge exchange cross-section is independent of energy. In the simulation the fields are quite non-linear particularly in asymmetric geometries and there are other effects such as field reversal at the electrode which could effect the distributions. The charge exchange cross-section for hydrogen decreases by an order of magnitude in going from 1 eV to 100 eV, which ions can quite easily do when crossing the sheath. Ions at low energies are therefore more likely to make a collision, which increases the probability of ions making more than one collision in the sheath. However the differences between the model and the simulation results are still puzzling since Wild and Koidl have obtained good agreement with experimental measurements using their model; and their distributions have been reproduced using planar PIC simulations (Surrendra and Graves (1990)) for similar dimensionless sheath conditions.

Another important parameter for etching which is effected by collisions in the sheath is the angular distribution of ions (IAD) arriving at the electrode – with broader IADs producing non-perpendicular etching. Figure 4.37 shows a plot of the IAD for $\alpha = 6$, $V_{rf} = 1$ kV and $p = 20$ mTorr. The angles are measured relative to the perpendicular to the electrode surface, so in the collisionless case ions all arrive at zero degrees. The live distribution has an spread of only a few degrees, indicating that most of the ions are coming in with small perpendicular energies relative to their parallel energies. The distribution at the grounded electrode is much broader, with a spread of up to 10°. The ions in the live sheath experience high average voltages and therefore gain large energies parallel to the field. This tends to narrow the distribution, and also means ions travel quickly through the sheath and so have a smaller likelihood of making collisions.

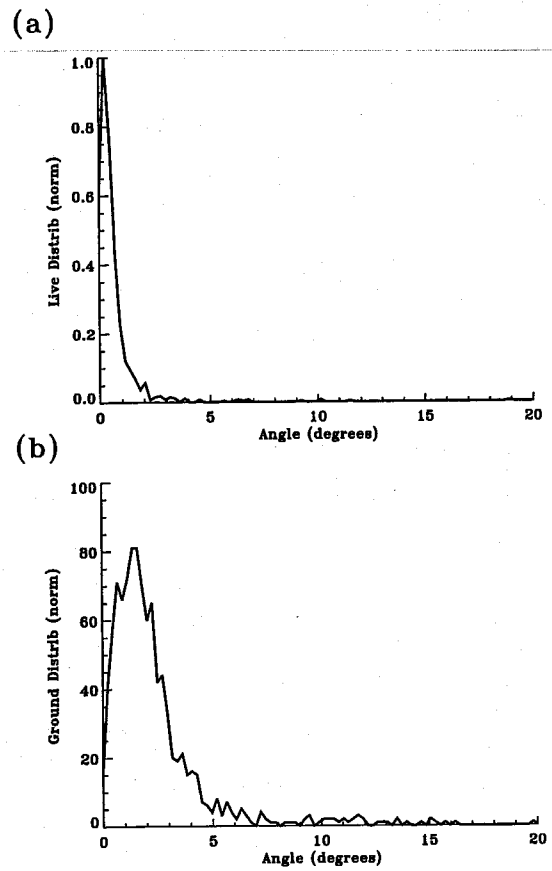

Figure 4.37 Angular distribution of ions at **(a)** live and **(b)** grounded electrode, for $\alpha = 6$, $p = 20$ mTorr.

The fields in the grounded sheath are smaller so the ratio of parallel to perpendicular energies is likely to remain higher, and as ions spend longer in the sheath they are more likely to have a collision.

Finally Figure 4.38 shows collisional ion trajectories through the sheath. Collisions are immediately obvious as abrupt changes in the ion energy. In a charge exchange collision ions transfer almost all their energy to the neutral, and so are immediately obvious as a decrease to 0 eV. The energy loss for elastic collisions on the other hand varies between 0 and 100 %, depending on the angle of collision, with an average loss of about 50 %. There are no obvious elastic collisions in the sample of ions plotted in Figure 4.38. This is not surprising, since the mean free path for elastic collisions is more than an order of magnitude larger than that for charge exchange, so ions are much less likely to make elastic collisions in the sheath. The ions appear to be spending between 4 to 5 cycles in the sheath although it is a little difficult to determine from this plot due to the added effects of collisions. The trajectories indicate that at

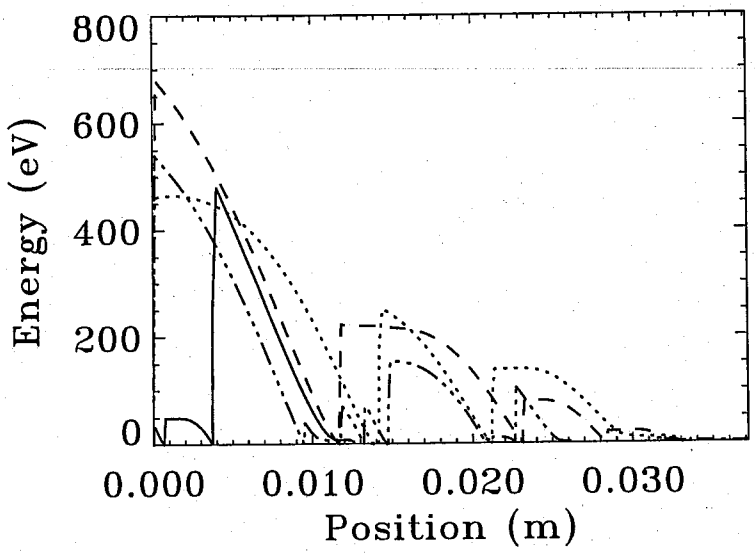

Figure 4.38 Collisional ion trajectories in the live sheath for α= 6, showing total energy as a function of position. The ion energy drops to zero when a charge exchange collision takes place. Only 4 ion trajectories are plotted.

20 mTorr the ions are making multiple charge exchange collisions in the sheath, as expected from the arguments given above. Note that fewer ions are plotted than for the collisionless case, for the sake of clarity.

4.7 Conclusion

This chapter has presented results for both collisionless and collisional ion simulations in asymmetric geometry. The sheath voltage ratio has been determined for a range of plasma parameters and is found to depend on the applied voltage and background gas pressure, as well as the electrode area ratio. This was not taken into account in the analytic expression derived by Lieberman (1989), nor is it commented on in other PIC simulations in asymmetric geometry (Alves *et al* (1991). An expression for the bias voltage has been determined as a function of the applied voltage, electrode area ratio and the ratio of the sheath densities, and a good approximation can be found by ignoring the differences in sheath density. The results from this expression agree well with results from the simulation.

Heating of electrons through interaction with the moving sheath edge is found to be critical in sustaining the discharge, as has previously been determined from planar simulations. However in the asymmetric system heating is found to occur almost

exclusively at the powered electrode sheath, due to asymmetry in the voltage distribution across the plasma. The power balance for the electrons was also examined and results from analytic expressions for sheath and ohmic heating of the electrons were found to agree with results from the simulation only for the symmetric case. The overestimation of ohmic heating by equation (4.20) has been related to high energy electrons in the bulk. The balance of power losses by the electrons through inelastic collisions and to the walls was found to agree well with the power gained by the electrons.

The sheath resistance was determined from the simulation using the ion power balance, and results were found to compare well to an analytic expression from Godyak *et al* (1991a). The relative power transferred to ions and electrons is found to depend on the total power absorbed by the plasma – at low values the power is divided equally between ions and electrons, while at high values more power goes into the ions.

Ion collisions on the simulation was found to substantially increase the plasma density and decrease the average ion energy. This is mainly due to reduced ion mobility in the collisional system. The IEDs at the electrodes are found to be dependent on both the rf field variation in the sheath and the number of collisions made by the ions in the sheath.